# Aerosol and Cloud Microphysical Characteristics of Rifts and Gradients in Maritime Stratocumulus Clouds

by

Tarah M. Sharon and Bruce A. Albrecht,

Division of Meteorology and Physical Oceanography, Rosenstiel School of Marine and Atmospheric Science, University of Miami, Miami, Florida

Haflidi H. Jonsson,

Center for Interdisciplinary Remotely Piloted Aircraft Studies, Marina, California

Patrick Minnis

Atmospheric Sciences Division, NASA Langley Research Center, Hampton, Virginia

Mandana M. Khaiyer

AS&M, Inc., Hampton, Virginia

Timothy Van Reken, John Seinfeld and Rick Flagan,

California Institute of Technology, Pasadena, CA

Corresponding author: Bruce A. Albrecht, Division of Meteorology and Physical Oceanography, Rosenstiel School of Marine and Atmospheric Science, University of Miami, 4600 Rickenbacker Causeway, Miami, Florida 33149; e-mail address: balbrecht@rsmas.miami.edu

**Abstract**

A cloud rift is characterized as a large-scale, persistent area of broken, low reflectivity stratocumulus clouds usually surrounded by a solid deck of stratocumulus. A rift observed off the coast of Monterey Bay, California on 16 July 1999 was studied to compare the aerosol and cloud microphysical properties in the rift with those of the surrounding solid stratus deck. Variables measured from an instrumented aircraft included temperature, water vapor, and cloud liquid water. These measurements characterized the thermodynamic properties of the solid deck and rift areas. Microphysical measurements made included aerosol, cloud drop and drizzle drop concentrations and cloud condensation nuclei (CCN) concentrations. The microphysical characteristics in a solid stratus deck differ substantially from those of a broken, cellular rift where cloud droplet concentrations are a factor of 2 lower than those in the solid cloud. Further, CCN concentrations were found to be about 3 times greater in the solid cloud area compared with those in the rift and aerosol concentrations showed a similar difference as well. Although drizzle was observed near cloud top in parts of the solid stratus cloud, the largest drizzle rates were associated with the broken clouds within the rift area. In addition to marked differences in particle concentrations, evidence of a mesoscale circulation near the solid cloud – rift boundary is presented. This mesoscale circulation provides a mechanism for maintaining a rift, but further study is required to understand the initiation of a rift and the conditions that may cause it to fill.

## 1. Introduction and Background

Clouds play a vital role in our global climate. Stratus and stratocumulus clouds, in particular, affect the climate system due to their spatial and temporal extent; stratus type clouds are observed over large fractions of the earth's surface for most of the year (e.g. Klein et al., 1995). Stratus, like most clouds absorb longwave radiation emitted by earth while emitting longwave radiation both to space and back to the ocean surface. This process involves the clouds absorbing longwave radiation energy emitted from the surface at a relatively warm cloud base and emitting it at slightly lower cloud top temperatures. Because low level stratiform clouds are not geometrically thick, they emit longwave radiation at about the same temperature as it is absorbed (Ramanathan et al., 1989). Thus the longwave radiation emitted back to space is not as significantly altered by these clouds as the shortwave radiation incident on the earth's surface.

Stratus decks off the coasts of California and other parts of the world, mainly off western boundaries of major continents, have been studied to better understand processes responsible for maintenance of these cloud decks. Features showing variability within stratus and stratocumulus clouds are important to study as well, because of their effects on the characteristics of stratus clouds themselves. For example, in Fig. 1 a rift observed off the coast of California has an albedo that is substantially less than the surrounding solid stratocumulus deck. In another case shown in Fig. 1b, the there is a strong enhancement of the reflectivity associated with ship tracks extending through a rift area observed just west of Monterey Bay California. Since rifts appear in areas of similar sea-surface, wind and temperature conditions as the adjacent solid cloud, they provide a unique opportunity for studying the processes that affect cloud structure.

The natural differences in aerosols and CCN concentrations between marine and continental air can result in substantial variability in the cloud characteristics. Drop size spectra associated with marine air, for example, have a much broader distribution than the spectra associated with continental air (Hudson and Yum, 1997). The effects of aerosols on the properties of stratus clouds can play a role in climate variability as well. Aerosols are the main source of particles on which cloud and fog droplets condense and affect solar radiation directly and through their influence on cloud albedo (Hoppel et al., 1990). Although exact effects are not fully quantified, the indirect effects of aerosols on climate include altering cloud albedo (Twomey, 1977) and changing precipitation efficiency (Albrecht, 1989). Cloud albedo is affected in the indirect effect where for a given liquid water content, a cloud with smaller, more numerous droplets has a higher albedo than one with larger but fewer droplets (Twomey, 1974). Further, modification of the droplet spectra by aerosol variations can in turn alter precipitation processes in the cloud and thus affecting cloud fraction. Both processes result in a decrease in solar radiation at the surface of the earth associated with an increase in aerosols.

Aerosols do not independently affect the microphysical characteristics of clouds. Precipitation processes influence aerosol concentrations and the drop size spectra in stratus clouds. For example, in precipitating boundary layer clouds, cloud condensation nuclei (CCN) spectra can be modified by collision and coalescence processes associate with drizzle, even if drizzle droplets do not reach the surface. In rifts, it is hypothesized that CCN concentrations may be reduced relative to those in the surrounding cloud and these lower CCN concentrations that may moderate cloud amount due to enhanced precipitation processes.

Although stratiform clouds play such an important role in global climate, other factors can affect large and mesoscale features in cloud properties. The rifts and ship tracks, shown in

Fig. 1, indicate the role that these features play. Although no formal definition exists as of yet, rifts are areas of low reflectivity that can be seen in satellite images of some stratus decks. These regions appear as broken cloud areas surrounded usually by more solid stratocumulus clouds with a noticeably different albedo than the rift area. The rifts often are associated with distinctly cellular conditions (Stevens et al., 2004), have lifetimes of days, and advect with boundary layer winds. Ship tracks, such as those shown in Fig. 1, however, exhibit enhanced reflectivity relative to the surrounding clouds (Durkee et al., 2000a, b) due to increased aerosols originating from ship exhaust and a reduction in drizzle (Ferek et al., 2000). Upon close inspection of the gradient area shown in Fig. 1, several ship tracks are seen to traverse the rift, two of which extend NW to SE and are crossed by a third trail extending almost E to W.

Rifts may also be good indicators of feedbacks between drizzle and observed cloud structure. If CCN concentration increases, clouds become more optically thick, as the collision and coalescence of cloud droplets is reduced due to increased concentrations of CCN, and the probability of precipitation decreases. This situation is consistent with areas of cloud enhancement along ship tracks (shown in Fig. 1b) where a smaller mean droplet size is observed (Albrecht, 1989). Hence, once drizzle begins, although the mechanism for initiation is not fully known, CCN are removed and the CCN spectra is modified by in-cloud scavenging, a process where water condenses on hygroscopic particles, and through collision and coalescence can fall as rain or drizzle. This cleansing process may lead to an optically less reflective area in which cloud lifetime decreases due to enhanced drizzle (Albrecht, 1989). If this process is operating, then cleansing process helps maintain conditions that further support drizzle formation.

The prevailing theory that explains rifts deals with differences in microphysical characteristics of the surrounding stratus deck. Several observations support this microphysical

theory (Stevens et al., 2004), although dynamics cannot be totally separated from the microphysical properties of clouds. Although research on these rift areas has been lacking, there has been considerable study of other aspects of marine stratocumulus clouds. Ship tracks are features that have been examined, and because ship tracks form due to emissions from ships, they may provide strong evidence for anthropogenic modification of clouds due to increases in CCN (Platnick et al., 2000).

By comparing and contrasting physical and thermodynamic properties of low albedo cloud areas of rifts with stratus clouds and ship tracks, it is hoped that theories applied to ship track formation can be analogously applied and tested using observations of rifts. It has been speculated that a complete knowledge of the characteristics of ship tracks will help quantify processes involved in anthropogenic aerosols and their role in increasing cloud reflectance, decreasing solar heating, and forcing local and global climate response (Albrecht, 1989). The same should be the case for rifts and gradients, though possibly for opposite effects: a decrease in cloud reflectance and an increase in the boundary layer and surface heating that affects local forcing on clouds and global climate.

One major difference between ship tracks and rifts, however, lies in the origins of each phenomenon. Ship tracks occur when increased emission of particles in the area of a ship plume leads to an increase in concentration of CCN and thus enhances the reflectivity of the ship plume and the resulting "ship track" is visible on satellite imagery (Hobbs et al., 2000; Durkee et al., 2000a, b; Ferek et al., 2000). Indeed, ships that produce more aerosols produce tracks that are brighter, wider, and longer-lived than those produced by ships that generate less aerosol (Durkee et al., 2000a, b). Thus ship tracks are produced by anthropogenic changes in aerosol

concentrations. Rifts, however, are due to natural variations--the origins of which are not yet known.

Several studies have focused on possible roles that dynamics play in development and maintenance of ship tracks (e.g. Hobbs et al., 2000; Durkee et al., 2000b; Frick and Hoppel, 2000; Platnick et al., 2000). Large-scale dynamics remained relatively the same both inside and outside of ship tracks; thus differences in dynamics have not been considered as a major source of uncertainty when dealing with characteristics of ship tracks. However, the same assumption cannot be made for cloud microphysics; therefore studies on ship tracks have focused on microphysical characteristics of ship tracks and differences between such tracks and the surrounding unmodified stratus clouds (Hobbs et al., 2000).

Since visually, rifts and gradients seem to be advected by winds associated with the large-scale dynamics of the surrounding regions, their irregular shape and appearance cannot be fully explained by the synoptic scale features present in the surrounding area. From a subjective analysis of satellite images of rift and gradient areas, rifts, when present, appear to encompass as much as 30 to 40 % of the large cloud areas over the eastern Pacific on average. In addition, some rifts appear as patchy areas of broken clouds, but they can also be thousands of km long and extend, in some cases, across the entire Pacific Ocean basin. Usually, rifts do not consist of completely clear air, but rather appear as areas of patchy, broken clouds, which have a cellular structure on the order of 10 – 20 km; these features will be referred to as mesoscale. Variations in cloud characteristics associated with rifts and the surrounding cloud areas provide laboratory-type conditions for studying processes responsible for affecting cloud characteristics.

Two unanswered questions related to stratus and stratocumulus clouds include: What causes embedded rifts and how are they able to sustain themselves? And more generally, what

effect does drizzle have on cloud structure? The major focus of this paper will be on the rift and how its microphysical and thermodynamic characteristics are similar and or different from those of the adjacent solid-clouded regions; a characterization of the variability in the microphysical characteristics and structure associated with rift areas observed in stratus off the coast of California.

The measurements used in this study were obtained from the Drizzle and Entrainment Cloud Study (DECS), conducted during the summer of 1999 on and off shore of Monterey Bay, California, which was designed to study stratus clouds and improve the representation of drizzle and entrainment in global and mesoscale models for quantitative simulation of the role of clouds in the climate system. Data for this study of embedded rifts and gradients in stratus and stratocumulus clouds were obtained from aircraft observations made during DECS. These data may contribute to our knowledge of rifts and effects of aerosol concentrations on such rifts and, consequently, to implications of their impact on climate.

**2. Experiment and Data**

An instrumented Twin Otter aircraft operated by the Center for Interdisciplinary Remotely Piloted Aircraft Studies (CIRPAS) through the Naval Postgraduate School in Monterey, California and California Institute of Technology was used to measure the characteristics of the boundary layer and stratocumulus clouds off the coast of California. The data used in this study were collected on a 16 July 1999 flight -- one of several flights made from 16 June through 22 July 1999. Measurements of rifts are not easily obtained from research aircraft flights due to limited range and an inability to predict where rifts might be observed in advance of any planned flights. On 16 July 1999, however, a rift was observed close enough to the shoreline along Monterey Bay, California, for the Twin Otter aircraft to reach it and obtain

measurements of the gradient area and the areas in and surrounding the rift. 16 July 1999 was the only such observation of rifts within reach of the Twin Otter during the entire DECS experiment.

For this study, instruments on the Twin Otter were used to observe aerosol and microphysical properties, and thermodynamic and dynamic variability of the marine boundary layer in and around the rift. Measurements from the Twin Otter included: aerosol, cloud, and drizzle droplet size distributions, CCN, radiative fluxes, winds, air temperatures, water vapor content, and sea surface temperatures. During the experiment, the aircraft was flown to sample boundary layer cloud properties as well as aerosol and environmental conditions above and below the stratocumulus cloud decks.

Instruments on the aircraft are summarized in Table 1, more detailed descriptions of the instruments can be found at: http://web.nps.navy.mil/~cirpas/. Instruments for characterizing thermodynamic properties included: a Rosemount sensor that measured air temperature, a chilled mirror device that measured dew point temperature, and a hot wire device that measured liquid water content. A Forward Scatter Spectrometer Probe (FSSP) measured size distribution of cloud-sized droplets. In addition, a Cloud Imaging Probe (CIP) was used to measure distribution of drizzle-sized droplets.

Particle distributions were obtained from a Cloud Aerosol Scatterprobe (CAS). The CAS probe measured aerosols, cloud droplets and drizzle-sized drops; for this study, the CAS probe was used to measure aerosols in the size range of 0.5 μm – 1 μm. CCN observations were made using a counter developed by Chuang et al. (2000) operated in single-supersaturation mode S of approximately 0.2%.

Smaller aerosol particles were characterized using an Ultrafine Condensation Particle Counter (CPC). The CPC was used to measure particles with diameters greater than 0.003 μm. By subtracting different count concentrations measured with the CPC, this probe was capable of identifying ultrafine particles, those falling in the size range of 3 nm – 7 nm, that are believed to be associated with new particle production.

The rift observed on 16 July 1999 was located off the western coast of California, centered around $36^0$ N and $126^0$ W. The gradient area moved toward the southwest at about 11 m $s^{-1}$. Figure 1b shows a rough outline of the rift from 1700 UTC to 2300 UTC, marking the progression of the gradient area. Through its lifetime, the rift appears to contract in the north – south direction. Surface winds for the case studied were from the north-northwest below the capping inversion and west-northwest to north-northwest above it. The southward movement of the rift shown in Fig. 1b is consistent with northerly winds in the area associated with low pressure systems inland and high pressure west of Monterey. The cellular nature of the region can also be seen in Fig. 1b. A subjective examination of this image indicates cellular structure on the order of 10 – 20 km.

Two types of sampling strategies were used to characterize cloud and boundary layer structure, and to compare to boundary layer, cloud and aerosol variability between the solid cloud and rift areas. Soundings provide vertical structure at selected locations in the solid stratus cloud and in the rift regime; constant height legs document horizontal variability between rift and non-rift areas. During a sounding maneuver, the CIRPAS Twin Otter aircraft during this flight made a vertical descent followed, usually, by a similar ascent.

There were 19 soundings obtained during the flight on 16 July 1999. All of these soundings were located just off the coast of California and to the east of the boundary between

the solid clouds and broken rift clouds observed in visible satellite images (see Fig. 1b). Nine of these soundings were obtained before the aircraft reached the solid portion of the stratus clouds, one sounding took place in the solid stratus clouds, and nine of the soundings were obtained on the flight track heading back to the coast.

Thermodynamic variables measured from the aircraft during vertical profiles and derived parameters calculated from these measured values characterized boundary layer structure that included a capping inversion. The structure below the inversion is used to examine the degree of mixing through the depth of the boundary layer. Cloud structure was obtained from vertical profiles of liquid water content (LWC) and cloud droplet distributions. These profiles allow for a comparison of cloud structure obtained in the rift and solid cloud region.

GOES visible satellite images, available about every 15 minutes while the aircraft was flying, provided characterizations of the larger scale cloud properties in the areas sampled by the aircraft. Vertical profiles from the aircraft are classified as either solid or broken by subjective analysis of the satellite images along the flight paths. Satellite images were also used to track temporal and spatial variations in the boundary between the solid and broken clouds. Further, these images were used to identify the times when the aircraft flew through the rift – solid deck boundary and to classify the aircraft observations as either solid stratus or rift measurements. In addition, satellite images were animated to track the progression of the rift through the day. Although these images do not capture nighttime conditions, they do show clearly the evolution of the rift during the day.

To illustrate the difference between the rift and solid cloud areas, soundings chosen for analysis include one in a solid cloud and thus having a well defined cloud structure that will be classified as “solid deck” or “deck”, one in a clear patch in the gradient area that will be called

"clear air rift" or "rift", and one in a small cloud contained within the rift that will be called "rift cloud". This provides a means for comparing similarities and differences between the rift and non-rift areas.

To analyze the microphysical characteristics of the clouds, aerosol concentration and cloud and drizzle droplet spectra data obtained from different probes were examined. However, because of the possibility of particle enhancements due to splashing on the aerosol inlet, CPC data were eliminated when the airplane was in clouds. During the level legs, the aircraft maintained a constant pressure altitude and flew lines across the boundary between the rift and non-rift region. Legs were flown at 100, 200, 400 and 700 m levels; only one pass at each level was conducted. The horizontal level legs were used to develop time-height sections through the rift–non-rift boundaries.

To provide a vertical section across the boundary, a time scale for each leg was developed to give a zero point at the location where the aircraft crossed the rift boundary (Table 2). Thus in the solid stratus area, time is negative and in the rift time is positive for the 4 layers flown. There is a short gap in the data at -5 min. on the 200-m flight leg due to the failure of the aircraft's data system during this time.

Downward solar radiation is also useful for defining the solid cloud-rift boundaries on each leg (Fig. 2). At 700 m small but clearly defined variability in downward solar radiation is associated with the stratus deck. At this level, about 30 m below cloud top, the aircraft likely traversed small upward protrusions in the solid deck. However, it is clear that this is not the case in the rift area as solar radiation is nearly constant, with the exception of small clouds that may have been penetrated near the end of the leg. Along the 400, 200 and 100 m legs there are well-defined signatures of the cloud in the downward solar radiation. At these levels solar radiation

associated with the solid stratus deck is substantially reduced from values near cloud top and shows relatively little variability (Fig. 2). In the area of the rift, however, there is substantially more variability. Cloud base height of the solid stratus deck is at about 400 m. As the deck is exited, downward solar radiation increases, with a relatively clear area within the rift area adjacent to the boundary. In the rift area, mesoscale patches of cloud are indicated by variability in shortwave that is consistent with the 10 - 15 km scale observed in the satellite images.

**3. Results**

The three distinct areas, the solid cloud deck, the clear air rift and the rift cloud, all show well-mixed potential temperature structure in the lower part of the boundary layer (Fig. 3a), below the capping inversion. The temperatures in the solid cloud are slightly lower than those in the rift area. Inversion heights for the three soundings fall range 740 m to 800 m and are slightly higher than the 710 +/- 75 m average for all 19 soundings conducted during the flight. Further, no significant differences in temperature between the solid cloud area and the rift area were observed along the horizontal legs (Fig. 3b). Sea surface temperature is variable across the horizontal level and shows no distinct change between the solid deck and broken rift area (not shown).

Water vapor mixing ratio (Fig. 3c), similarly, shows a fairly well mixed structure, although evidence of a sub-cloud layer / cloud layer stratification is observed. The boundary layer mixing ratios in the solid deck are slightly lower than those in the clear air rift and the rift cloud, which have similar values in the sub-cloud layer. The mixing ratios measured along the horizontal legs (Fig. 3d) show similar cloud-rift differences with the subcloud layer mixing ratios in the rift area about 0.5 g/kh higher than those beneatht the solid cloud deck. Mesoscale variability of the mixing ration at 100 m appear to be associated with evaporation in the vicinity

of drizzle patches. But evaporation alone may not be associated with these moisture variations since equivalent potential temperature $\theta_e$ observed on the 100 m leg also shows mesoscale variability. There is some variability in the mixing ratios observed above the boundary layer with values just above the inversion capping the solid deck about 0.5 g/kg less than those over the rift. Thus, the broken nature of the clouds in the rift area cannot be explained by the entrainment of dry air into the boundary layer, since the mixing ratio just above the inversion is slightly higher than those in the stratus deck.

Wind speeds (Fig. 4a) in the boundary layer are similar in both the rift and cloud deck area with values of about 7 m $s^{-1}$ below the inversion; this speed is consistent with advection of the stratus clouds and rift in the GOES satellite image (Fig. 1a, b). Although the decrease in wind speed over the solid deck is not as large as that over the rift area, this difference in wind speed is not significant. In addition, wind direction (not shown) below the inversion is from the north-northwest for all three soundings. The winds shift above the inversion to more west-northwesterly above the solid deck (above 700 m) and more northerly (at about 1000 m) above the rift regime.

The wind variations shown by the horizontal legs (Fig. 4b) are consistent with the profiles. There are no significant decreases or increases in the wind speed across the rift boundary, although wind speed decreases slightly beneath the cloud when moving from the solid stratus deck into the broken rift area and it increases slightly at the cloud top layer. Average wind speed in the boundary layer is about 6 m $s^{-1}$. Wind speeds along the horizontal legs at 200 and 400 m indicate mesoscale variability in the rift cloud region, particularly at time (t) = + 6 min. where a mesoscale cloud patch is observed. Winds tend to be weaker in this area. Wind

direction (not shown) through all the layers remains at near a constant northerly to north-northwesterly direction, again consistent with the profiles.

Although there are some differences between the solid deck and the rift regime in both wind speed and direction above the base of the inversion, the wind shear does not appear to contribute in any substantial way to the dynamics of the boundary layer. Since the rift moves at about the same speed and direction as the boundary layer winds, the area above inversion, which is moving in a more westerly direction, does not seem to be a factor in maintaining the rift structure within the stratus deck. Further, most of the apparent differences between the solid deck and the rift regime occur below the base of the capping inversion.

The concentrations of the ultrafine particles are used to mark areas of new particle formation (Fig. 5a, b, c). In the solid stratus (Fig. 5a), ultrafine particle counts remain close to zero below the cloud layer. Above the cloud, however, concentrations of the smallest particles peak to average of about 200 $cm^{-3}$, while particles ranging in size from 7 to 12 nm remained close to zero. Profiles in the clear air rift area (Fig. 5b), however, show that the smallest particles have a substantial peak of about 1350 $cm^{-3}$ just below the inversion. There is a double peak in the concentration of 3 to 7 nm particles just below the inversion in the clear air rift profile. Particles ranging in size from 7 to 12 nm are also greater than zero, peaking at nearly 500 $cm^{-3}$. The high concentration of the smallest particles indicates new particle production was active during the evolution of the cloud-rift boundary areas.

Similar to the clear air rift profile, measurements made around the rift cloud (Fig. 5c) also indicate significant concentrations of ultrafine particles. Just below the inversion of the rift cloud, the concentration of particles from 3 to 7 nm peaks at more than 2000 $cm^{-3}$. As in the clear air rift, a dual peak appears near the base of the capping inversion. However, the multiple

peaks are not obvious since the data are edited to remove in-cloud values. Concentrations of ultrafine particles associated with the rift cloud appear larger than those in the clear air. In addition, there is another peak in the concentration of ultrafine particles just above the ocean surface in the rift cloud profile, with the smallest particles reaching a concentration of about 1000 $cm^{-3}$, which is substantially greater than those under the solid deck and in the clear air rift.

The ultrafine particle concentrations shown in the profiles are confirmed by observations along the horizontal flight tracks (Fig. 5 d). Ultrafine particle concentrations were uniformly low at the lowest. At 200 m and 400 m, however, ultrafine concentration spiked at time t = 7 min in the rift area. New particle production was particularly notable in the clear air near the tops of the mesoscale cloud area in the rift at 700 m. Another distinct area of high concentrations of the smallest of the ultrafine particles was the cloud free area adjacent to deck-rift boundary. This high concentration of ultra fine particles, and simultaneous dearth of large particles at 700 m suggests that there is new particle production occurring at the edge of the solid stratus deck.

A summary of aerosol and cloud properties sampled on this flight is given in Tables 3, 4 and 5. Areas analyzed for these tables include 100-m segments from the profiles and 30-sec. segments from the horizontal legs. Levels selected for this analysis were chosen to encompass the sub-cloud layer, the base of the cloud, and the top of the cloud. Times selected for the leg values were 30-sec. segments chosen to represent three areas in the cloud-rift area as follows: - 1 min. to - 0.5 min. represents the deck area, 0 min. to + 0.5 min. is the clear rift area and + 5 min. to + 5.5 min. is the rift cloud.

Ultrafine particle concentrations underneath the rift cloud in the profile are far greater than those under the deck and the rift profile (Table 3). Ultrafine concentrations from the legs in the sub cloud layer are lowest underneath the rift cloud. Although in the sub cloud layer the

greatest ultrafine concentration observed along the legs is located under the solid deck, in the lower cloud this maximum concentration is associated with the rift (Table 4). In addition, the rift has a minimum in cloud drop concentrations, which is consistent with the lack of cloud in this area. Ultrafine particle concentrations in the upper cloud layer (Table 5) are greatest in the rift cloud profile and the leg associated with the deck. Concentrations of ultrafine particles in the rift profile are about 8 times larger than in the deck profile. This is consistent with possible new particle production, as smaller particles would coagulate into larger particles if both groups were present in the same area.

Aerosol concentrations in the sub-cloud layer (Table 3) are small and relatively invariant for all three areas. In the lower cloud layer (Table 4), aerosol concentrations are greatest in the deck area. They are 1.5 to 3 times greater than those in the rift cloud. Aerosol concentrations in the rift profile are an order of magnitude less than those in the deck, while the ultrafine particle concentrations are 2 times greater in the rift than in the deck.

CCN concentrations, the most relevant quantity for cloud production, have substantial variations across the rift. There is a dramatic difference between the solid stratus deck and embedded rift area. All of the CCN counts in the solid stratus area ($t < 0$) are about 3 times greater than those in the rift at all levels (Fig. 6). The lowest CCN concentrations are observed near the top of the boundary layer in the rift area. At this level entrained air with low CCN concentrations was sampled along with the cloudy air. On the other legs in and below the cloud, CCN drops markedly across the deck to rift transition. Although this air mass taken as a whole is considered "clean marine air" with concentrations of ~ 50 $cm^{-3}$ of CCN, low concentrations of ~ 10 $cm^{-3}$ of CCN in the rift area would be considered nearly pristine air. This variability

appears to be a critical factor for explaining differences between the stratus deck and embedded rift region.

CCN concentrations in the sub-cloud layer (Table 3) are substantially greater under the deck than under the rift and the rift cloud, although the clear air rift concentrations are greater than those in the rift cloud. CCN concentrations in the solid deck are greater than those in the rift or in the rift cloud at the lower cloud layer (Table 4). In the upper cloud layer (Table 5), CCN concentrations are generally low, with the greatest of 15 $cm^{-3}$, located in the rift cloud regime.

A hot wire sensor measured cloud liquid water structure in the solid deck and rift regime (Fig. 7a). The profile associated with the solid stratus deck shows a well-defined structure, with liquid water increasing from the cloud base towards cloud top, spiking at cloud top, and then decreasing sharply above the cloud. The rift liquid water profiles are much more variable than the well-defined cloud structure found in the solid stratus cloud deck. In the lower layer of the cloud, liquid water content in the solid deck closely follows the adiabatic liquid water content. The deviation of liquid water content from the adiabatic liquid water values near cloud top may be due to either drizzle processes occurring in the cloud at this level or cloud top entrainment tending to dry the cloud areas near the top of the boundary layer. The sounding in the clear air shows no cloud water. The rift cloud profile falls somewhere between the two extremes. It indicates the presence of clouds, but the structure is not that of a “classic” cloud profile. This shows the variability of clouds that are present in the rift area compared with the solid cloud profile. The cloud located within the rift is also a shallower cloud than the solid cloud and it does not have a structure like that observed in the solid cloud; it also has two peaks, centered at about 500 m and 600 m that could be artifacts of the way in which the rift cloud was traversed by

the aircraft. Because the aircraft cannot make a pure vertical ascent or descent, it travels about 2 to 3 km in the horizontal direction; thus it may have crossed parts of different or the same cloud area while making the sounding.

Cloud liquid water content for the constant height legs flown at 100, 200, 400 and 700 m (Fig. 7b), further indicates the solid nature of the cloud in the deck and the more broken nature in the rift. Thus the area under the stratus deck is quite homogeneous, while the area in the rift exhibits patchy variability in liquid water content. The patchy variability in liquid water content is associated with smaller lower clouds that are penetrated during this level flight leg. At 200 m, there is patchy area of cloud liquid water measured in the rift at t = +5 min; drizzle may be associated with this cloud and the associated evaporation would be consistent with the increase in mixing ratio and a lower cloud base height in this area. The leg at 700 m shows the most significance between the two regions. It is evident that a well-defined cloud is present in the stratus region as indicated by liquid water content. As expected, the liquid water drops to zero in the clear area just past the rift boundary. Patchy clouds within the rift have maximum water contents that are similar in magnitude to liquid water values in the solid cloud region. The bases of clouds in the rift area are lower than those in the deck as indicated by liquid water signatures at 200 m. These mesoscale cloud patches are also visible in satellite images of the rift (Fig. 1a, b).

The cloud droplet concentrations are substantially higher in solid stratus the profile associated with the solid stratus cloud deck than in the small rift cloud element sampled at 500 m (Fig. 8a). Most of these droplets are found within the cloud layer with concentrations between 40 $cm^{-3}$ and 60 $cm^{-3}$ and decrease near cloud top (see Tables 3 and 4). However, the average drop concentration is about 20 $cm^{-3}$ in the rift cloud compared with about 40 $cm^{-3}$ in the solid

cloud deck. The profile of droplet concentrations through the clear air of the rift is close to zero by definition. Near cloud top at 700 m there are higher cloud droplet concentrations within the stratus deck than are associated with the rift region (Table 5).

Consistent with locations of the largest droplet concentration, FSSP-measured effective volume diameter, or volume weighted mean diameter, of the cloud drops increases from cloud base to cloud top in the solid deck (Fig. 8b). This increase in effective volume diameter is consistent with the increase in liquid water (Fig. 7a) and a nearly constant number concentration (Fig. 8a). In the region where the concentration of droplets decreases near cloud top, the particle size increases. The rift cloud, however, does not show the same structure. Effective diameters in the rift cloud particles are slightly greater than those of the solid deck, especially in the lower cloud layer -- consistent with smaller droplet concentrations in the lower cloud layer.

At 700 m (Fig. 8c), where the drop concentrations in the rift are smaller than in the deck, the size of particles in the two areas is similar at about 20 μm. The envelope of effective diameter at 400 m associated with the solid deck is about 15 μm and about 20 μm in the rift. At 200 m and 100 m, the droplets in the patchy drizzling clouds are not very numerous and have a large effective diameter of about 20 μm. These fewer, larger droplets yield a water content similar to that resulting from the more numerous smaller droplets in the deck cloud.

Precipitation-sized droplets measured with the CIP are also highly variable. The solid deck profile shows some drizzle drops located below the cloud -- consistent with drizzle falling to the surface. Concentrations (not shown) of drizzle sized droplets within the deck increase near cloud top to a maximum of about 2000 liter$^{-1}$. This increase in drizzle concentrations near the top of a cloud is consistent with a well-developed cloud. The rift cloud exhibits two spikes in the

same location as the liquid water content spikes of the hot-wire-sensor (Fig. 7a), with concentrations just above 4000 liter$^{-1}$.

Drizzle sized concentrations (not shown) for the level legs are similar. At about 700 m, drizzle droplets were observed near cloud top in the mesoscale cloud region in the rift with concentrations, ~ 5000 liter$^{-1}$, similar to those in the deck profile of about 5000 liter$^{-1}$. The highest concentrations located at the edge of the solid stratus deck could be consistent with the formation of larger droplets in an updraft area in the solid cloud. This is also consistent with most of the drizzle drops located at about cloud top in the drizzle liquid water profile. The drizzle in the rift area, where drizzle drop concentrations are similar to those found in the solid stratus cloud, is at t = 5 min. At 400 m, there are small drizzle concentrations at t = 2.5 min and t = 5 min past the boundary, but the drop concentrations at this level are close to 0. At 200 m, measurable concentrations occur beneath the mesoscale cloud area in the rift (t = 5 min). Similarly, at 100 m, there is a slight spike in drizzle drop concentrations at t = 5 min. There is also an area near the rift-cloud boundary where concentrations are slightly greater than 0.

As expected, drizzle drop effective diameters (Fig. 9a, b) are considerably larger than the collocated cloud droplets. At 700 m, drizzle drop effective diameter is relatively consistent through the level. At 200 m, however, effective diameter of drizzle drops in the rift area is greater than that under the stratus deck. Effective diameter under the stratus clouds is slightly less than 100 μm, whereas that associated with the rift peaks at almost 200 μm. This difference is consistent with concentrations, since there are relatively few, but larger, drizzle drops under the rift in the mesoscale cloud area (t = 5 min). This concentration-size relationship is also evident at 100 m where slight deviations from zero in drop concentrations are associated with effective diameters of about 150 μm.

Drop distribution spectra obtained in the deck and the rift cloud areas are shown in Fig. 10. These spectra were obtained in and below the cloud and summarize the previous results. The spectrum for the rift cloud clearly shows the increased drizzle contributions relative to the deck cloud spectra. The rift cloud drop spectrum is broader than that of the solid deck and, despite the gap, appears to be bimodal further supporting the distinct differences in the cloud microphysics and aerosol characteristics between the solid deck and the rift regime. The concentrations of 80 μm droplets are similar for both cloud areas. At 150 μm, however, the concentrations in the rift cloud and below the cloud increase substantially, particularly in the drizzle observed below the actual cloud.

**4. Discussion**

The in situ measured differences in microphysical properties together with the changes in the cloud field evident in the satellite imagery suggest that the rift is an eroded area of a formerly continuous stratus deck. It is possible that the rift originally evolved from drizzling portions of the solid deck. In the solid deck, the proportion of drizzle droplets is insufficient to erode the deck while, in the rift, the proportion is insufficient to maintain the deck.

The results clearly show marked differences in the microphysical characteristics of the clouds in these two distinct stable areas, while there are no significant differences in their thermodynamic characteristics. Ultrafine particle concentrations are greatest just below the inversion in the clear rift profile while they are at a minimum in the deck profile area. This could be an area of possible new particle formation. It coincides with the lack of larger particles that otherwise would provide surface area for condensation and prevent new particle formation. CCN concentrations associated with the increase in concentrations of ultrafine particles indicates the lack of larger particles in the area and thus clean air with respect to the surrounding

conditions. Further, CCN concentrations associated with the deck area are about 3 times greater than those in the rift area where the concentrations drop.

These results also suggest that mesoscale processes may be involved in keeping air in a very pristine state in the deck–rift areas. Figure 11 provides a schematic of how one such process may work. The updraft shown in the idealized model symbolizes a process whereby precipitation forms near the top of the solid cloud at the edge of the stratus cloud and is connected to an outflow area characterized by very clean air as indicated by reduced CCN concentrations. Outflow near the cloud top also provides a mechanism by which cleaner air is pumped into the rift allowing for areas having the potential for new particle production – or areas containing aerosols that are much too small to be CCN. The sub-cloud inflow from the rift side into the edge of the stratus deck would reduce the average number of CCN while providing the same amount of water vapor. This kind of process would increase the drizzle rate at the edge of the deck causing the deck to erode around the rift. In the absence of strong advective and radiative efforts, the process would be self-sustaining until the deck was completely broken up. Other factors, like the diurnal cycle in solar radiation absorption that tends to dissipate the deck (e.g. Blaskovic et al., 1991) presumably would enhance the erosion process during the day. At night, the rift should tend to fill as minimal solar absorption allows for more effective drizzle. Within the rift area, cumulus cells would continue to form and drizzle out in the absence of any substantial concentrations. At night the drizzle process may be enhanced as the cloud layer deepens.

Although the data are insufficient to document fully the dynamics associated with the stratus deck region and rift areas, microphysics seems to dominate these areas. A large-scale picture of the cloud droplet sizes is available in the satellite analyses. The radiative effective

droplet diameter Deff was derived from the GOES-10 data using the methods of Minnis et al. (1995, 1998) every half hour during the flights. Deff is roughly 1.33 times greater than the volume effective diameter reported earlier. The distribution of Deff at both 1900 UTC (Fig. 12a) and 2100 UTC (Fig. 12b) clearly show the rift areas as regions with Deff values greater than about 35 μm. The solid deck areas around the rifts typically have values of 26 to 35 μm, while those for the clouds farther south away from the rift areas range from 14 to 22 μm. Figure 12 and similar images for other hours during the day indicate that much of the aircraft-sampled rift was gradually divided into smaller sections apparently as a result of the criss-crossing ship tracks that are evident as nearly linear features of reduced Deff in Fig. 12. Obviously, the introduction of additional aerosols from ships and from the continental air alters the microphysical structure of the rift clouds and may contribute to a reduction of drizzle and a brightening of clouds in rift areas.

The *in situ* data show that the number of drizzle droplets increasing from the deck into the rift corresponds to a rise in Deff. Although the values of Deff in the rift and in much of the solid deck area are unrealistically large, the correspondence to the in situ drizzle data suggests that Deff could be used as a drizzle index that would be invaluable for studying the development and filling of the rifts. Beyond that, these unique in situ data show that the droplet size distributions in these areas are broader and include more drizzle-sized droplets than the modified gamma distributions typically used for retrieving cloud droplet sizes from satellite data (e.g., Minnis et al. 1998). The added drizzle droplets, which are strong absorbers of the near-infrared radiation used to retrieve droplet size, could explain why the retrieved values of Deff are so large. Thus, in addition to shedding light on a potential new tool for the estimation of drizzle intensity, in situ data like those analyzed here, will be useful for refining algorithms to retrieve

cloud properties. A complete understanding of the processes maintaining and dissipating the marine stratus decks requires knowledge of the large-scale context, which is only available from satellite data.

Although there have been limited previous studies that focus on the characteristics within rift areas, a review of published studies of drizzle in marine stratocumulus clouds indicates a tendency for these clouds to be observed in rift areas. Albrecht et al. (1985), for example, study a broken area of stratocumulus clouds (13 June 1976) off the coast of California where drizzle was observed (Brost et al., 1982a, b). These observations were made in a low reflectivity rift area (see Fig. 2 of Albrecht et al., 1985) and indicate cloud droplet concentrations of about 45 $cm^{-3}$ compared with about 125 $cm^{-3}$ observed in a solid cloud deck 4 days later. During the First ISCCP Regional Experiment (FIRE 1987), there were several well-documented cases when drizzle from stratocumulus was observed (Austin et al., 1995) in clouds located off the coast of California. The clouds studied in one of these cases, 30 June 1987, are shown in Fig. 1a. On this day, the UK Met Office C-130 and the NCAR Electra flew a coordinated mission to study downstream boundary layer evolution. The C-130 and Electra were serendipitously located separately in adjacent areas of a solid cloud deck and a rift as shown in Fig. 1a. A detailed comparison of the thermodynamic and wind structure revealed little difference between the two areas, other than a more strongly decoupled boundary layer in the rift area than in the solid cloud. Substantial differences were observed, however, in the cloud microphysical characteristics as shown in Fig. 13. Cloud droplet concentrations in the rift cloud were about 40 – 50 $cm^{-3}$ compared with about 150 $cm^{-3}$ in the solid cloud. The mean volume radius for these two regimes is about 20 – 22 μm in the rift cloud compared with 16 μm in the solid cloud (Fig. 13). Drizzle rates were estimated to be about 0.5 – 1 mm $day^{-1}$ in the rift compared with near-

zero drizzle rates in the solid cloud. The microphysical conditions documented in these previous studies are clearly consistent with those in our current study and further support our hypothesis that drizzle processes are critical in the processing of aerosols and the maintenance of rift clouds that have low cloud droplet concentrations and a strong propensity to maintain conditions conducive to drizzle formation.

**5. Concluding Remarks**

Environmental conditions lend themselves to several feedbacks that influence the existence of clouds and affect their characteristics and properties. In the case of stratus and stratocumulus clouds, drizzle mechanisms in the deck area are not always sufficient to deplete the area of cloud water, thus the stratus deck is able to persist. If drizzle mechanisms are such that the clouds drizzle out, or deplete cloud water in the stratus area, it is possible that a rift may form. In addition, in the rift areas, drizzle seems to be more efficient than the solid stratus deck in suppressing increased CCN concentrations, thus prohibiting the stratus deck from maintaining a solid sheet over the entire area. The introduction of non-marine aerosols would aid the persistence of the deck.

In general, aerosols have a significant impact on clouds and climate. These impacts are consistent with indirect aerosol effects. More specifically, the second indirect aerosol effect that relates increases in cloud lifetime to decreases in drizzle due to smaller cloud drops. This effect is seen in ship tracks that tend to be more reflective in gradient areas due to susceptibility for indirect effects in the rift regime. The marked differences that aerosols produce are seen in rifts and ship tracks. Decreased albedos are a sign of the rift and gradient areas where drizzle processes appear to deplete the aerosol concentrations, while the increased reflectivity in ship track clouds belies the addition of anthropogenic aerosols to the marine boundary layer.

A relatively simple mechanism has been proposed here for maintaining a rift, but the perturbation that initiates a rift or the conditions that lead to the filling of a rift remains a mystery. Further study is required to fully understand the marine stratus rift areas. In addition to testing the hypothesis for rift maintenance, such future studies should include research on the formation of rift regimes as well as dissipation of rifts to determine how they form and why they dissipate. The development of improved satellite algorithms for quantifying drizzle in conjunction with other cloud characteristics is needed along with in situ data and a detailed cloud process model. In situ observations including turbulence and radiation data are needed for more days when rifts are present in stratus decks. In addition to tracking long-lived rifts, the satellite data should provide a more global perspective on the frequency of occurrence of rifts, the extent of their influence, and their macroscopic characteristics and variability. That information together with more detailed in situ data is needed to realistically account for rifts in marine stratus clouds and their role in the aerosol indirect effect.

The results in this study provide direct evidence of indirect aerosol effects associated with natural variability in the cloud characteristics. More specifically, these results provide evidence of the second indirect aerosol effect that relates increases in fractional cloudiness to decreases in drizzle associated with higher CCN concentrations. Decreased albedos and more open cellular structures characterize the rift and gradient areas where drizzle processes work to diminish CCN concentrations. The ship tracks observed within the rift observed during in this study indicate the susceptibility for indirect effects in rift areas areas. Evidence for air that has been cleansed of all CCN by cloud process is evident in the observations presented. The presence of natural long-lived variations in marine stratocumulus cloud associated with the naturally forming rift areas and man-induced ship tracks clearly supports a the theory of bi-stable CCN and cloud states

(Baker and Charlson, 1989) and provides convincing evidence of the importance of the second aerosol indirect effect. Since cloud rifts can affect extensive areas of the Earth's extensive stratocumulus decks, it is important to understand the physical mechanisms that cause these areas to form initially, since these mechanisms may be closely tied to other components the climate system.

Acknowledgements: This research was supported under NSF Grant ATM-9902416. The efforts of Dr. Phil Durkee in directing the aircraft to the rift area studied are greatly appreciated. Hal Maring is thanked for his valuable assistance with the interpretation of the new particle production. Additionally, we wish to thank Kirk Ayers for assistance with analyzing the satellite data. The satellite analyses were supported by NOAA Agreement NA00AABRG0330 under the PACS Program.

**References**


Albrecht, B. A., 1989: Aerosols, cloud microphysics, and fractional cloudiness. *Science*, **245,** 1227-1230.

Albrecht, B.A., R. S. Penc, W. S. Schubert, 1985: An observational study of cloud-topped mixed layers. *J. Atmos. Sci.*, **42,** 800-822.

Austin, P., Y. Wang, V. Kujala, and R. Pincus, 1995: Precipitation in stratocumulus clouds: Observational and modeling results. *J. Atmos. Sci.*, **52,** 2329-2352.

Baker M. B., and R. J. Charlson, 1989: Bistability in CCN concentrations and thermodynamics in the cloud-topped boundary layer. *Nature*, **345**, 142-144.

Blaskovic, M., R. Davies, and J. B. Sirider, 1991: Diurnal variation of marine stratocumulus over San Nicolas Island during July 1989. *Mon. Wea. Rev.*, **117,** 1469-1478.

Brost, R.A., D. H. Lenschow, and J.C. Wyngaard, 1982a: Marine stratocumulus layers: Part I: Mean conditions. *J. Atmos. Sci.*, **39,** 800-817.

Brost, R.A., J.C. Wyngaard, and D. H. Lenschow, 1982b: Marine stratocumulus layers: Part II: Turbulence budgets. *J. Atmos. Sci.*, **39,** 818-836.

Chuang, P. Y., A. Nenes, J. N. Smith, R. C. Flagan, and J. H. Seinfeld, 2000: Design of a CCN instrument for airborne measurement. *J. Atmos. Oceanic Technol*., **17**, 1005-1019.

Durkee, P.A., R.E. Chartier, A. Brown, E. J. Trehubenko, S.D. Rogerson, C. Skupniewicz, K. E. Nielsen, S. Platnick, and M. D. King, 2000a: Composite ship track characteristics. *J. Atmos. Sci.*, **57,** 2542 2553.

Durkee, Philip A., K. J. Noone, and R. T. Bluth, 2000b: The Monterey Area Ship Track experiment. *J. Atmos. Sci.*, **57,** 2523-2541.

Ferek, R. J., T. Garrett, P. V. Hobbs, S. Strader, D. Johnson, J. P. Taylor, K. Nielsen, A. S. Ackerman, Y. Kogan, O. Liu, B.A. Albrecht, and D. Babb, 2000: Drizzle suppression in ship tracks. *J. Atmos. Sci.*, **57,** 2707-2728.

Frick, G. M. and W. A. Hoppel, 2000: Airship measurements of ship's exhaust plumes and their effect on marine boundary layer clouds. *J. Atmos. Sci.*, **57,** 2625-2648.

Hobbs, P. V., T. J. Garrett, R. J. Ferek, S. R. Strader, D. A. Hegg, G. M. Frick, W.A. Hoppel, R. F. Gasparovic, L. M. Russell, D. W. Johnson, C. O'Down, P. A. Durkee, K. E. Nielsen, and G. Innis, 2000: Emissions from ships with respect to their effects on clouds. *J. Atmos. Sci.*, **57,** 2570-2590.

Hoppel, W.A., J.W. Fitzgerald, G. M. Frick, R. E. Larson, and E. J. Mack, 1990: Aerosol size distributions and optical properties found in the marine boundary layer over the Atlantic Ocean. *J. Geophys. Res.*, **95,** 3659-3686.

Hudson, J. G. and S. S. Yum, 1997: Droplet spectral broadening in marine stratus. *J. Atmos. Sci.*, **54,** 2642-2654.

Klein, S. A., D. L. Hartman, and J. R. Norris, 1995: On the relationships among low-cloud structure, sea surface temperature, and atmospheric circulation in the summertime northeast Pacific. *J. Climate*, **8,** 1140-1155.

Minnis, P., D. P. Garber, D. F. Young, R. F. Arduini, and Y. Takano, 1998: Parameterization of reflectance and effective emittance for satellite remote sensing of cloud properties. *J. Atmos. Sci.,* **55,** 3313-3339.

Minnis, P., D. P. Kratz, J. A. Coakley, Jr., M. D. King, D. Garber, P. Heck, S. Mayor, D. F. Young, and R. Arduini, 1995: Cloud optical property retrieval (Subsystem 4.3). "Clouds and the Earth's Radiant Energy System (CERES) Algorithm Theoretical Basis Document, Volume III: Cloud analyses and radiance inversions (Subsystem 4)", *NASA RP 1376 Vol. 3*, edited by CERES Science Team, pp. 135-176.

Platnick, S., P.A. Durkee, K. Nielsen, J. P. Taylor, S. C. Tsay, M. D. Knig, R. J. Ferek, P. V. Hobbs, and J. W. Rottman, 2000: The role of background cloud microphysics in the radiative formation of ship tracks. *J. Atmos. Sci.*, **57,** 2607-2624.

Ramanathan, V., R.D. Cess, P. Harrison, P. Minnis, B. R. Barkstrom, E. Ahmad, and D. Hartmann, 1989: Cloud-radiative forcing and climate: Results from the Earth Radiation Budget Experiment. *Science*, **243,** 57-63.

Stevens, B., G. Vali. K. Comstock, R. Wood, M.C. van Zanten, P.H. Austin, C.S. Bretherton, and D. Lenschow, 2004: Pockets of Open Cells (POCs) and Drizzle in Marine Stratocumulus. Bull. Amer. Meteor. Soc. (Submitted).

Twomey, S., 1977: The influence of pollution on the shortwave albedo of clouds. *J. Atmos. Sci.*, **34,** 1149-1152.

Twomey, S., 1974: Pollution and planetary the albedo. *Atmos. Environ.*, **8,** 1251-1256.

# Figure Legends

Figure 1. (a) GOES Satellite Image of stratus clouds and embedded rift observed off the coast of California, 30 June 1987 1845 UTC. (b) GOES visible Satellite Image of stratus clouds and embedded rift observed off the coast of California, 16 July 1999 1700 UTC with progression of rift shown by the dashed (corresponds to 1700 UTC) and solid thick line (corresponds to 2300 UTC). Flight path is also overlaid to identify location of soundings and path of aircraft. The circles indicate the location of the soundings taken during the flight (the light circles were not analyzed in detail in this study, the dark circles indicate the three soundings analyzed in detail).

Figure 2. Downward solar radiation measured along level legs during flight on 16 July 1999. The vertical gray line indicates the border between the solid stratus deck and the rift region.

Figure 3. (a) Potential Temperature profiles for solid deck, clear air rift and rift cloud. The black diagonal lines indicate the Moist Adiabatic Lapse Rate, (MALR). The dashed gray lines roughly mark cloud top and cloud base. (b) Potential temperature for the horizontal legs at ~100 and ~200 m. The vertical gray line indicates the border between the solid stratus deck and rift region. (c) Mixing ratio profiles. The dashed gray lines roughly mark cloud top and cloud base.

Figure 4. Wind Speed (a) for the profiles of the solid deck, clear air rift and rift cloud. The gray dashed line indicates the average inversion for the three profiles. (b) across the horizontal legs. The vertical gray line indicates the border between the solid stratus deck and rift region.

Figure 5. Ultrafine particle profiles for (a) Solid Deck, (b) Clear air rift and (c) Rift Cloud. The black line indicates the average inversion height for the three profiles. The vertical gray line indicates the border between the solid stratus deck and rift region. In cloud measurements made in clouds have been omitted due to instrument limitations under cloud conditions.

Figure 6. CCN concentrations for the four level legs. The vertical gray line indicates the border between the solid stratus deck and rift region. In cloud measurements made in clouds have been omitted due to instrument limitations under cloud conditions.

Figure 7. (a) Liquid water content for profiles. The horizontal dashed gray lines roughly mark cloud top and cloud base of the solid cloud. The gray line indicates the Moist Adiabatic Lapse Rate (MALR). (b) Liquid water content across the level legs. The vertical gray line indicates the border between the solid stratus deck and rift region.

Figure 8: (a) Effective diameter for cloud droplets in solid cloud and rift cloud areas. The dashed gray lines roughly mark cloud top and cloud base of the solid cloud. (b) Drizzle Drop concentrations in the solid cloud (circle) and rift cloud (diamond) areas. The

dashed gray lines roughly mark cloud top and cloud base of the solid cloud. (c) Effective diameter for cloud droplets along the level legs. The vertical gray line indicates the border between the solid stratus deck and rift region.

Figure 9: (a) Effective diameter for drizzle drops in the cloud profiles. The horizontal dashed gray lines roughly mark cloud top and cloud base of the solid cloud. (b) Effective diameter for cloud drops along the four horizontal legs. The vertical gray line indicates the border between the solid stratus deck and rift region.

Figure 10: Cloud and drizzle droplet spectra from the solid cloud deck (solid line) and the rift cloud (dotted line) regions. These spectra are based on approximately 5 sec averages. The cloud spectra were obtained at a height of about 75 m. Drizzle spectra were made below the cloud (at 75 m) in the two areas. The first bin of the drizzle spectra was eliminated due to instrument error of over counting the number of droplets (thus the gap in data between the cloud and drizzle drop spectra).

Figure 11: Schematic of possible cleaning mechanism associated with stratus deck.

Figure 12: Radiative effective cloud droplet diameter derived from GOES-10 data off the coast of California during 16 July 1999 at (a) 1900 UTC and (b) 2100 UTC.

Figure 13. Cloud microphysical differences from C-130 (solid cloud) and Electra (rift area) aircraft measurements made during 30 June 1987.

Figure 1. (a) GOES Satellite Image of stratus clouds and embedded rift observed off the coast of California, 30 June 1987 1845 UTC. (b) GOES visible Satellite Image of stratus clouds and embedded rift observed off the coast of California, 16 July 1999 1700 UTC with progression of rift shown by the dashed (corresponds to 1700 UTC) and solid thick line (corresponds to 2300 UTC). Flight path is also overlaid to identify location of soundings and path of aircraft. The circles indicate the location of the soundings taken during the flight (the light circles were not analyzed in detail in this study, the dark circles indicate the three soundings analyzed in detail).

1(a)

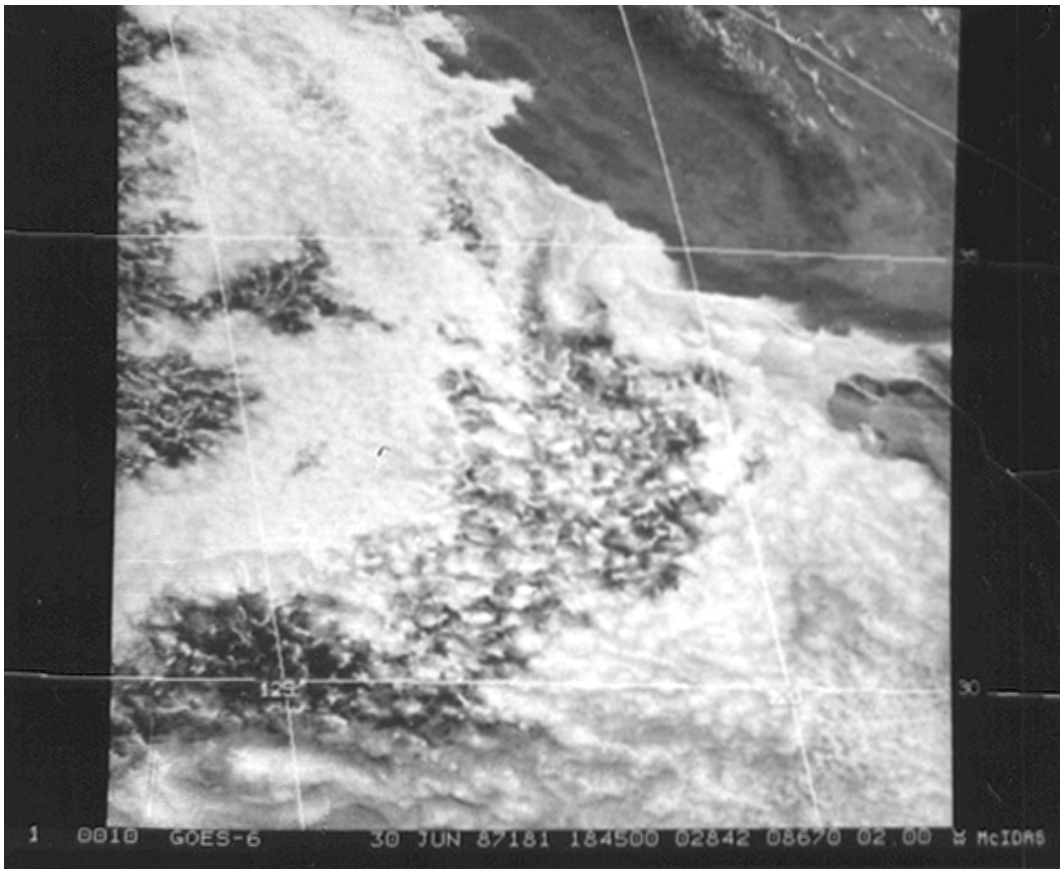

1(b)

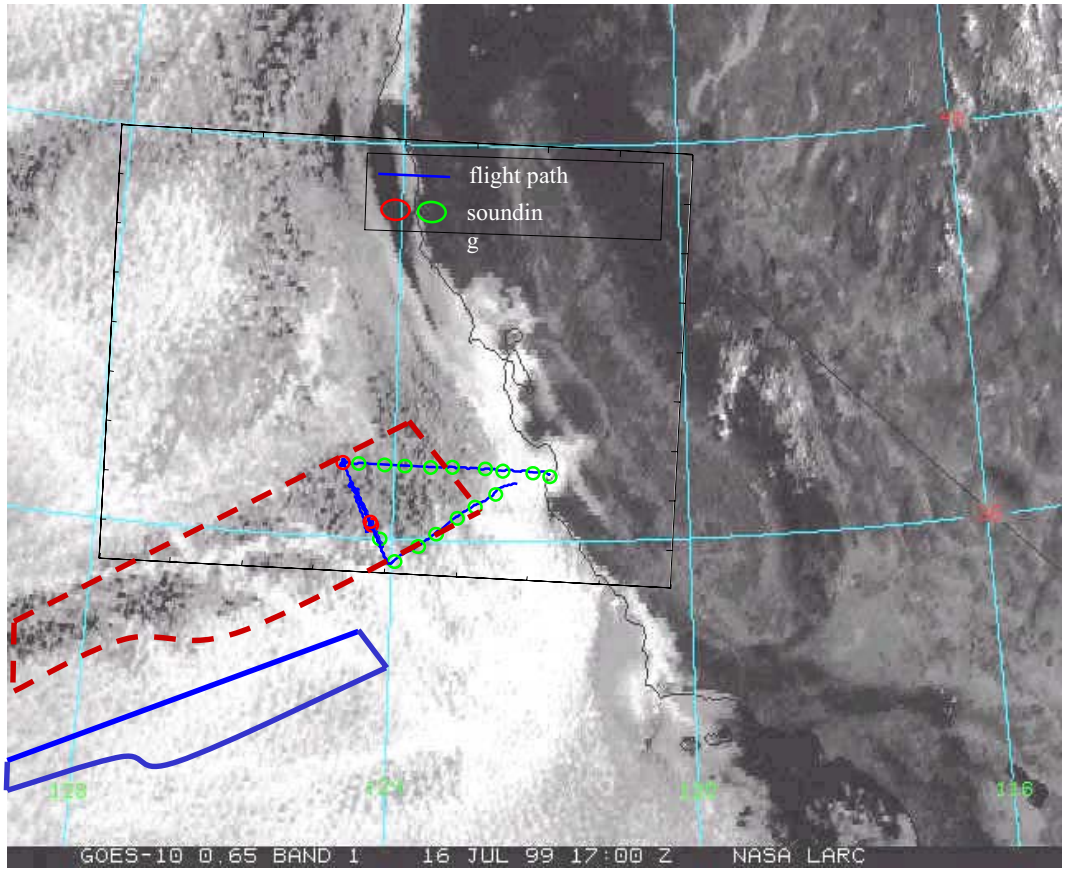
flight path
soundin
g
GOES-10 0.65 BAND 1 16 JUL 99 17:00 Z NASA LARC

Figure 2. Downward solar radiation measured along level legs during flight on 16 July 1999. The vertical gray line indicates the border between the solid stratus deck and the rift region.

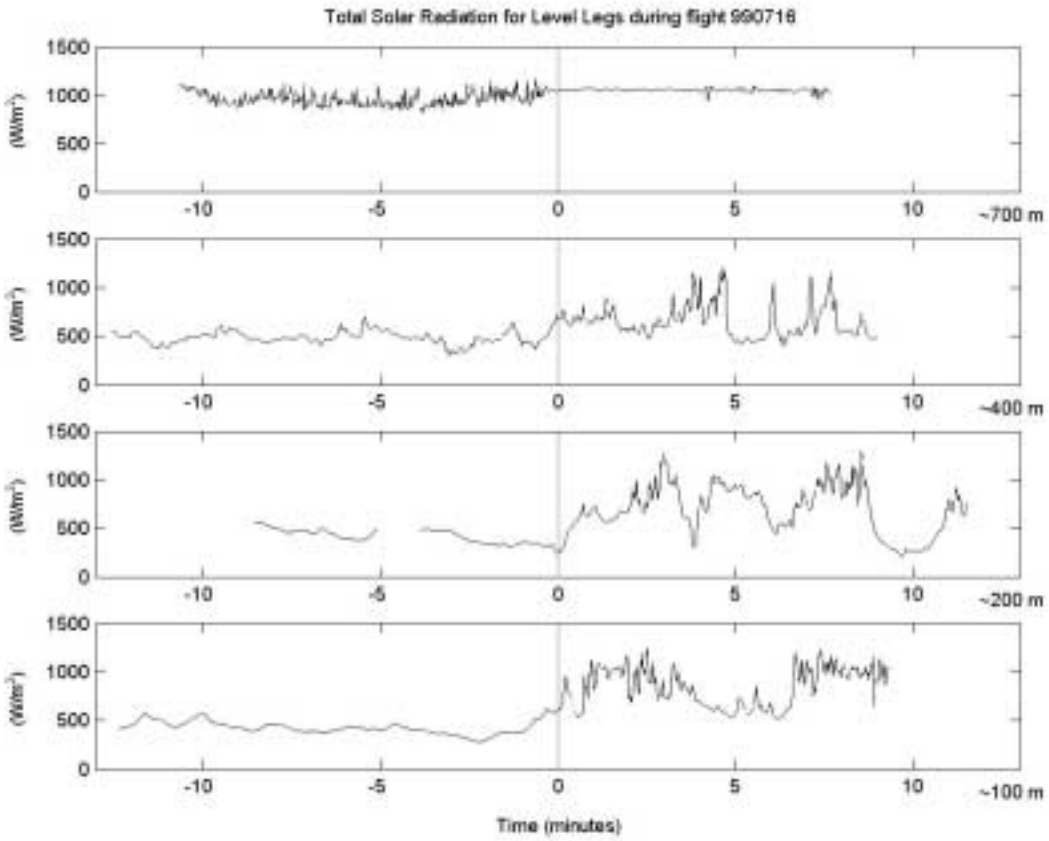

Figure 3. (a) Potential Temperature profiles for solid deck, clear air rift and rift cloud. The black diagonal lines indicate the Moist Adiabatic Lapse Rate, (MALR). The dashed gray lines roughly mark cloud top and cloud base. (b) Potential temperature for the horizontal legs at ~100 and ~200 m. The vertical gray line indicates the border between the solid stratus deck and rift region. (c) Mixing ratio profiles. The dashed gray lines roughly mark cloud top and cloud base. (d) Mixing ratio for the horizontal legs at ~100 m, ~ 200 m, ~400 m and ~ 700 m. The vertical gray line indicates the border between the solid stratus deck and rift region.

3(a)

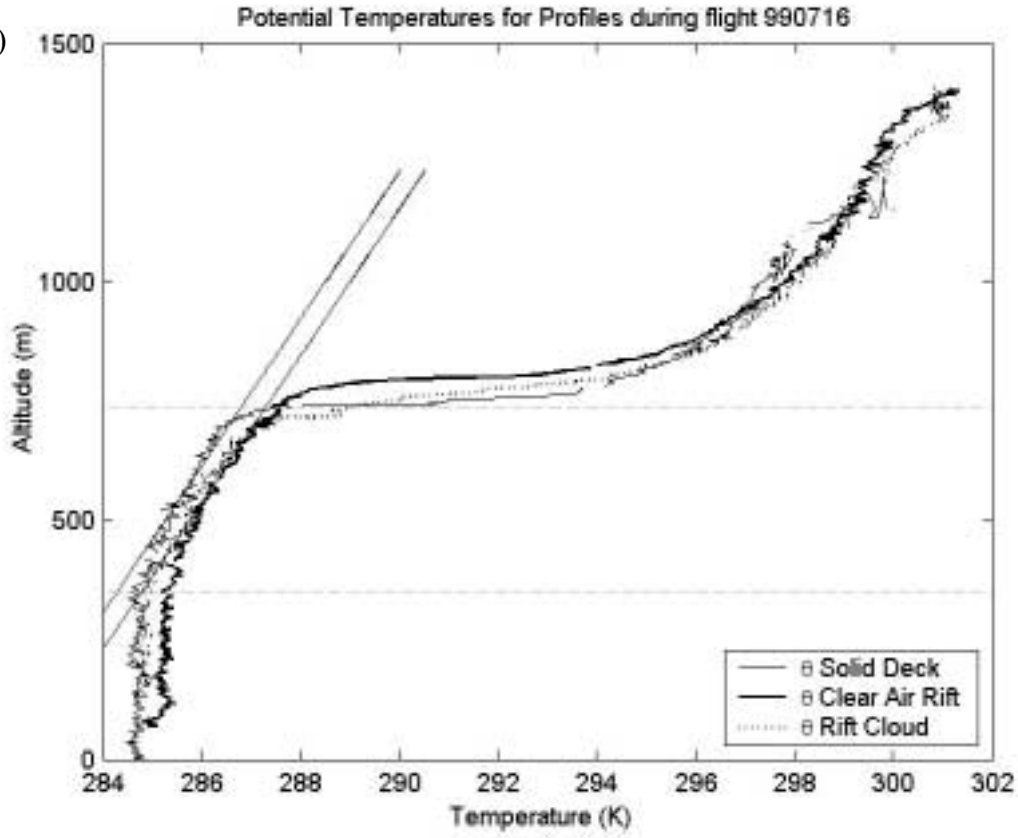

3(b)

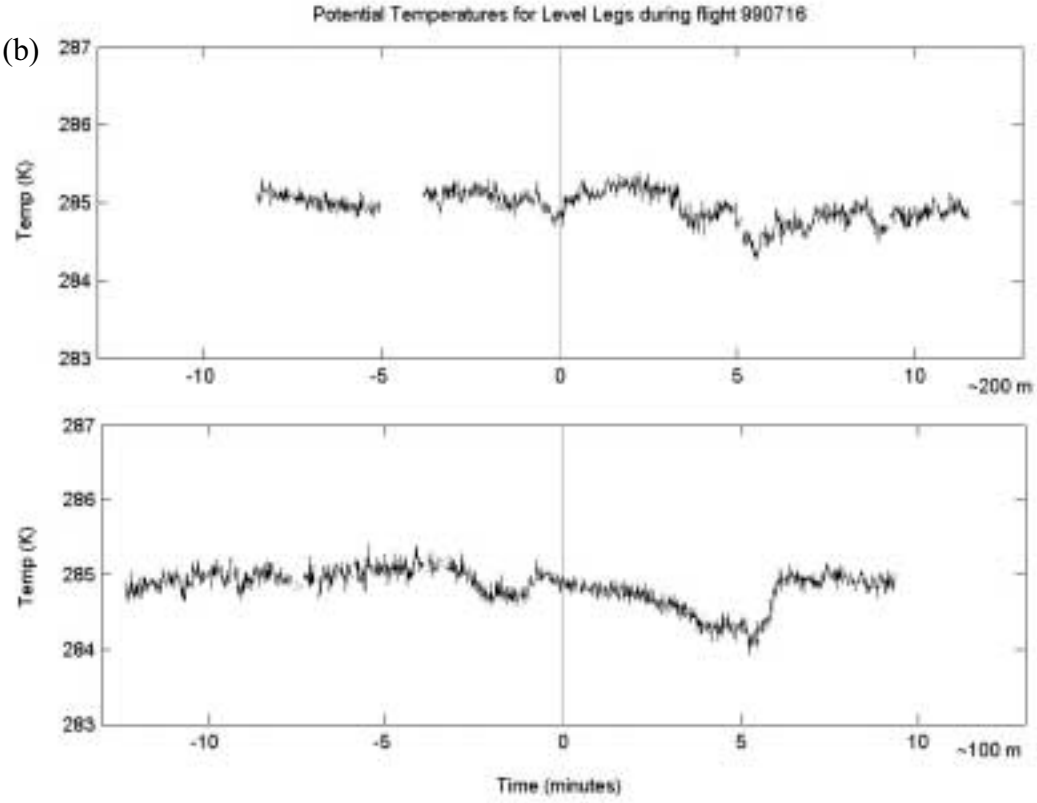
Potential Temperatures for Level Legs during flight 990716
Temp (K)
287
286
285
284
283
-10
-5
0
5
10
~200 m
Temp (K)
287
286
285
284
283
-10
-5
0
5
10
~100 m
Time (minutes)

3(c)

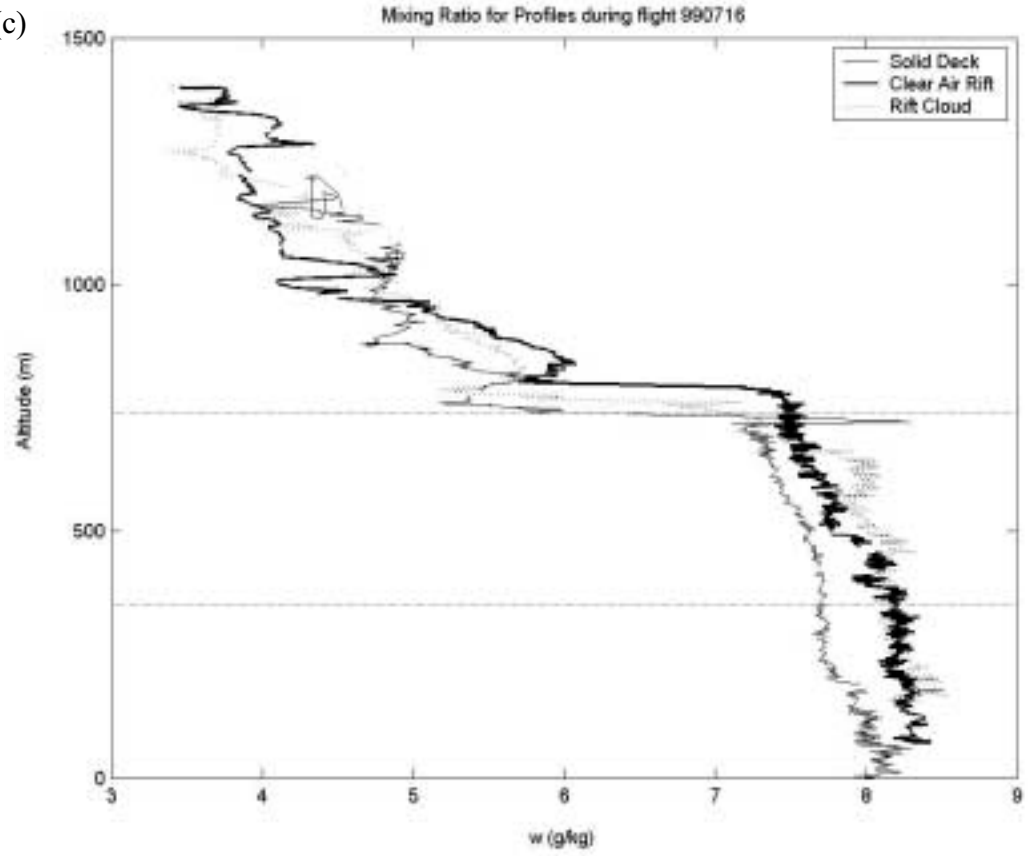
Mixing Ratio for Profiles during flight 990716
Solid Deck
Clear Air Rift
Rift Cloud
Altitude (m)
1500
1000
500
0
3
4
5
6
7
8
9
w (g/kg)

3(d)

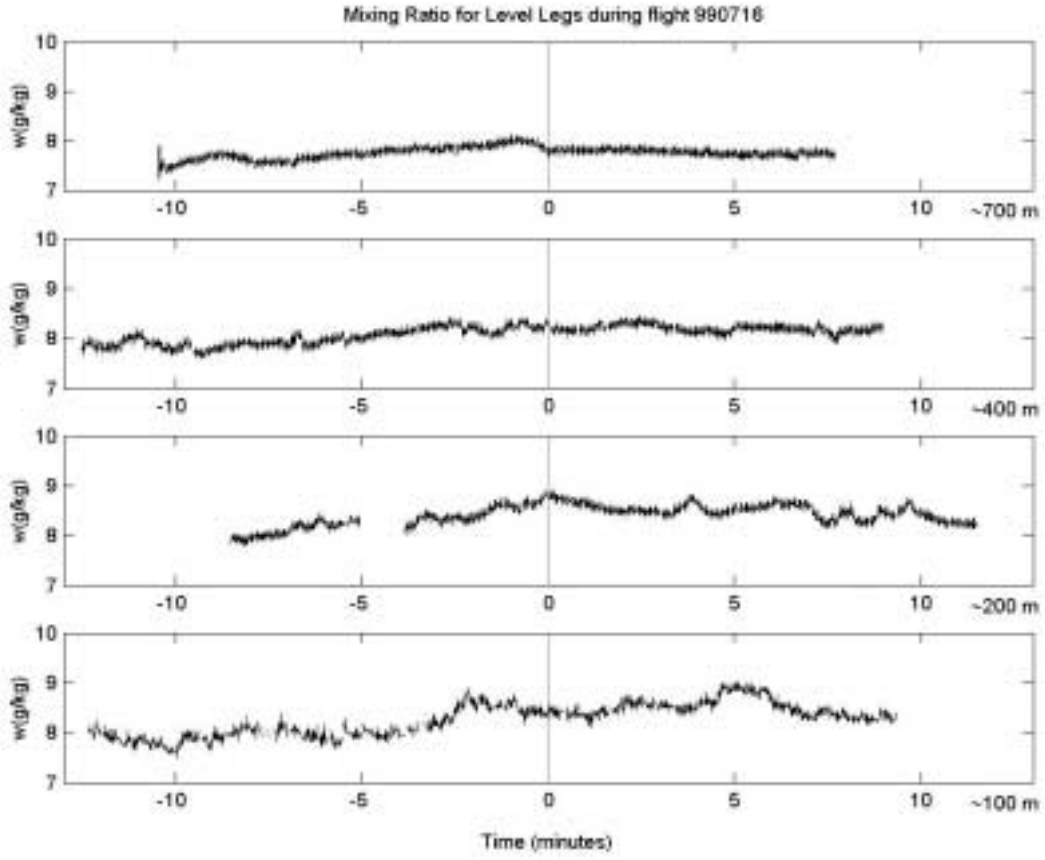
Mixing Ratio for Level Legs during flight 990716
w(g/kg)
10
9
8
7
-10
-5
0
5
10
~700 m
~400 m
~200 m
~100 m
Time (minutes)

Figure 4. Wind Speed (a) for the profiles of the solid deck, clear air rift and rift cloud. The gray dashed line indicates the average inversion for the three profiles. (b) across the horizontal legs. The vertical gray line indicates the border between the solid stratus deck and rift region.

4(a)

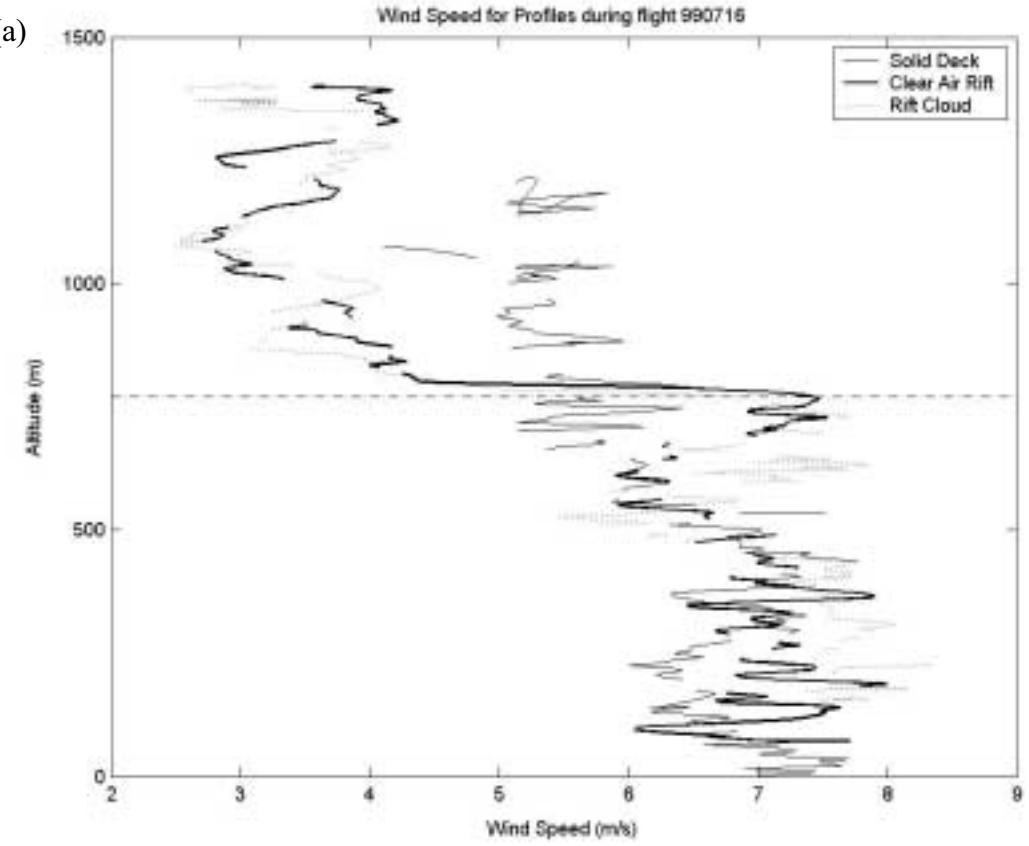

4(b)

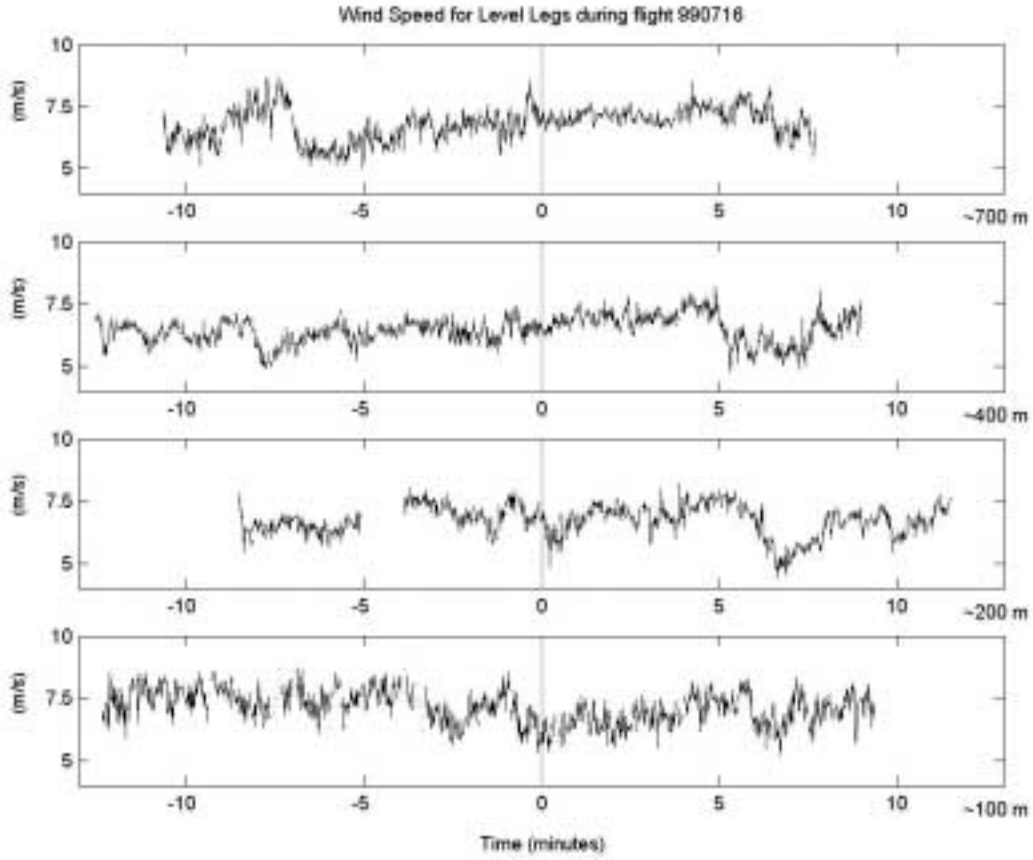
Wind Speed for Level Legs during flight 990716
(m/s)
10
7.5
5
-10
-5
0
5
10
~700 m
~400 m
~200 m
~100 m
Time (minutes)

Figure 5. Ultrafine particle profiles for (a) Solid Deck, (b) Clear air rift and (c) Rift Cloud. The black line indicates the average inversion height for the three profiles. The vertical gray line indicates the border between the solid stratus deck and rift region. In cloud measurements made in clouds have been omitted due to instrument limitations under cloud conditions.

5(a)

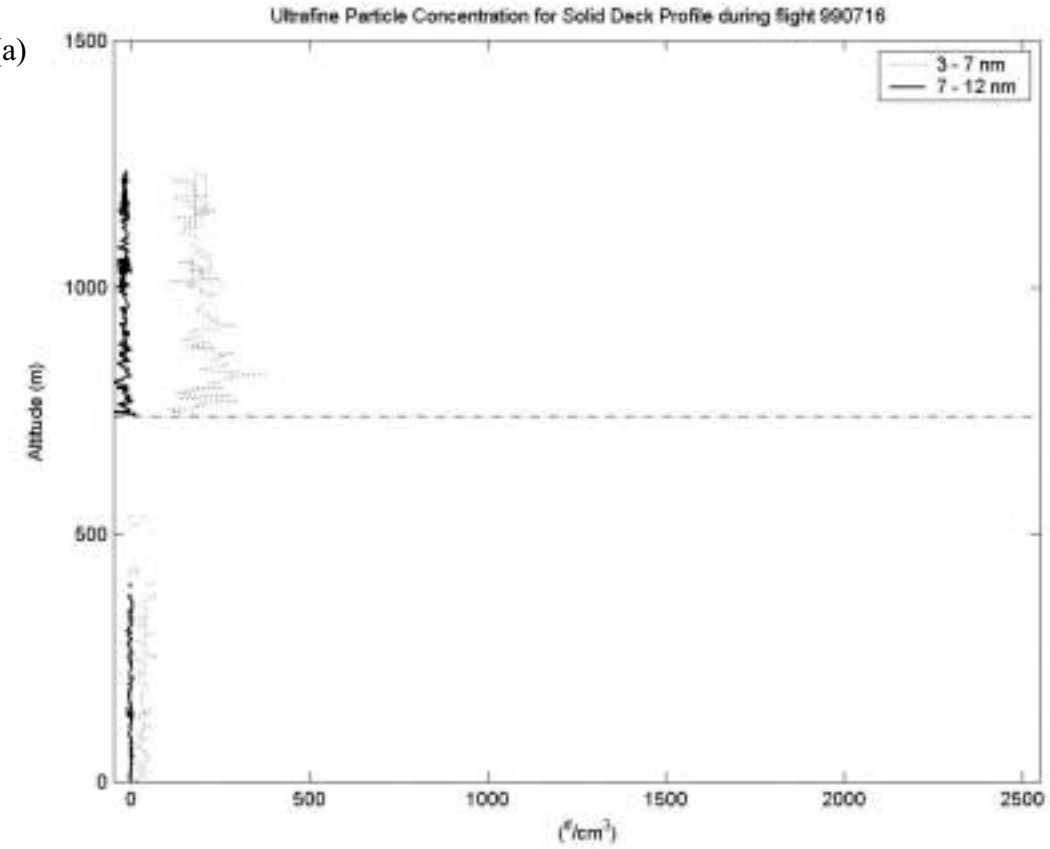

5(b)

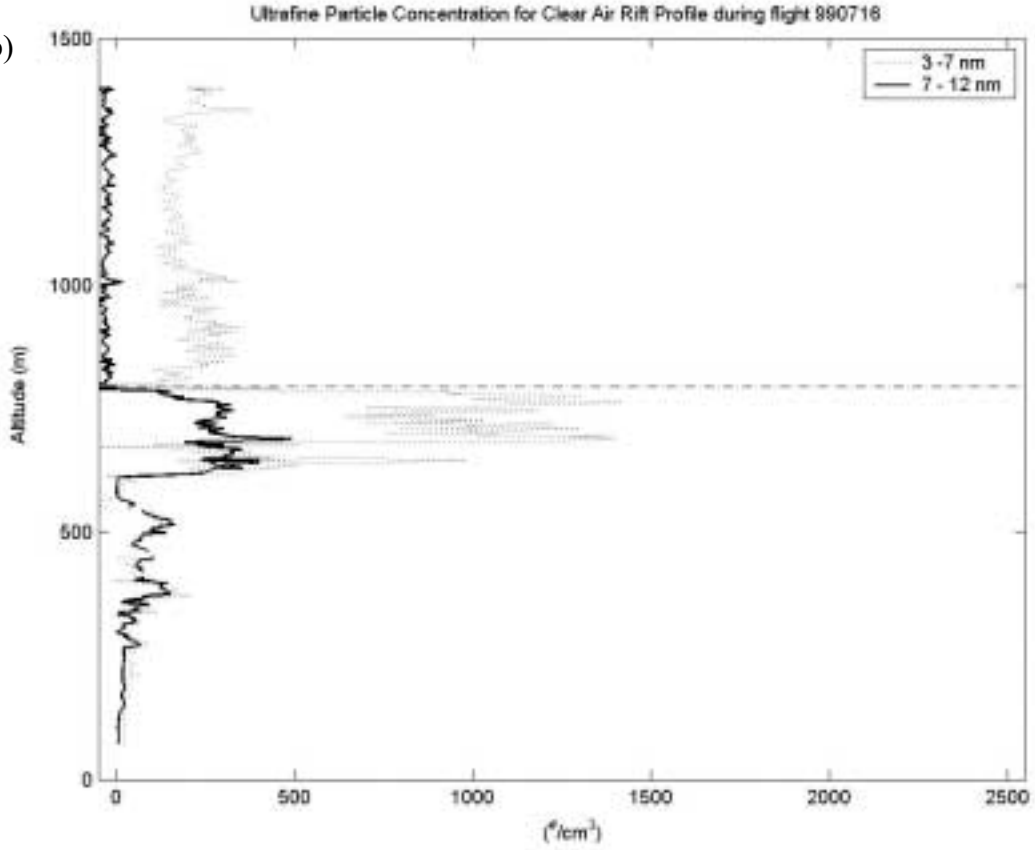
Ultrafine Particle Concentration for Clear Air Rift Profile during flight 990716
3 - 7 nm
7 - 12 nm
Altitude (m)
1500
1000
500
0
0
500
1000
1500
2000
2500
(#/cm³)

5(c)

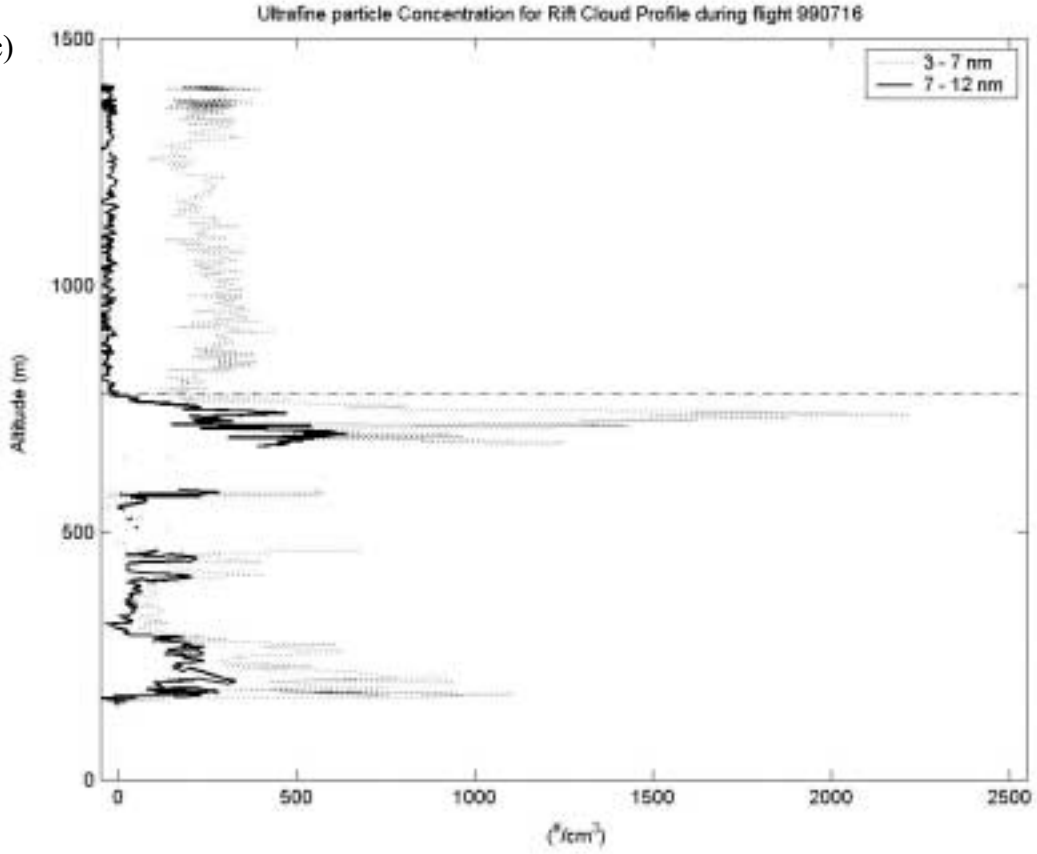
Ultrafine particle Concentration for Rift Cloud Profile during flight 990716
3 - 7 nm
7 - 12 nm
Altitude (m)
1500
1000
500
0
0
500
1000
1500
2000
2500
(#/cm³)

5(d)

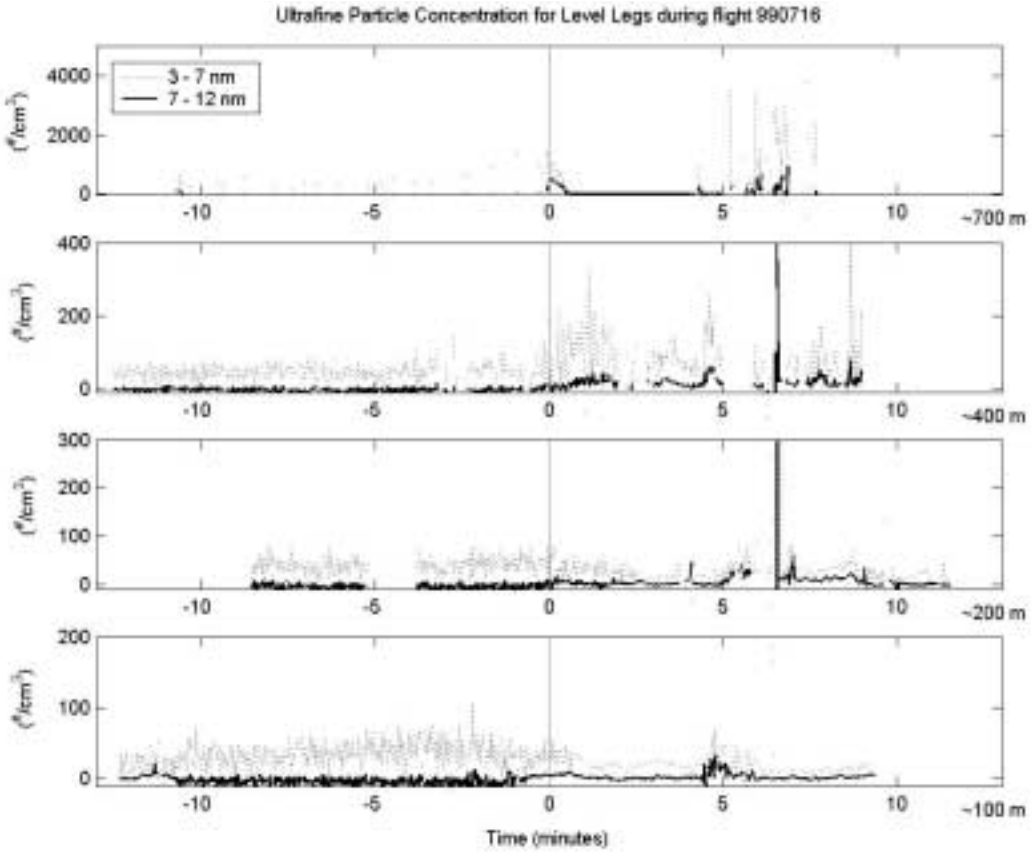
Ultrafine Particle Concentration for Level Legs during flight 990716
3 - 7 nm
7 - 12 nm
4000
2000
0
400
200
0
300
200
100
0
200
100
0
-10
-5
0
5
10
~700 m
~400 m
~200 m
~100 m
Time (minutes)

Figure 6. CCN concentrations for the four level legs. The vertical gray line indicates the border between the solid stratus deck and rift region. In cloud measurements made in clouds have been omitted due to instrument limitations under cloud conditions.

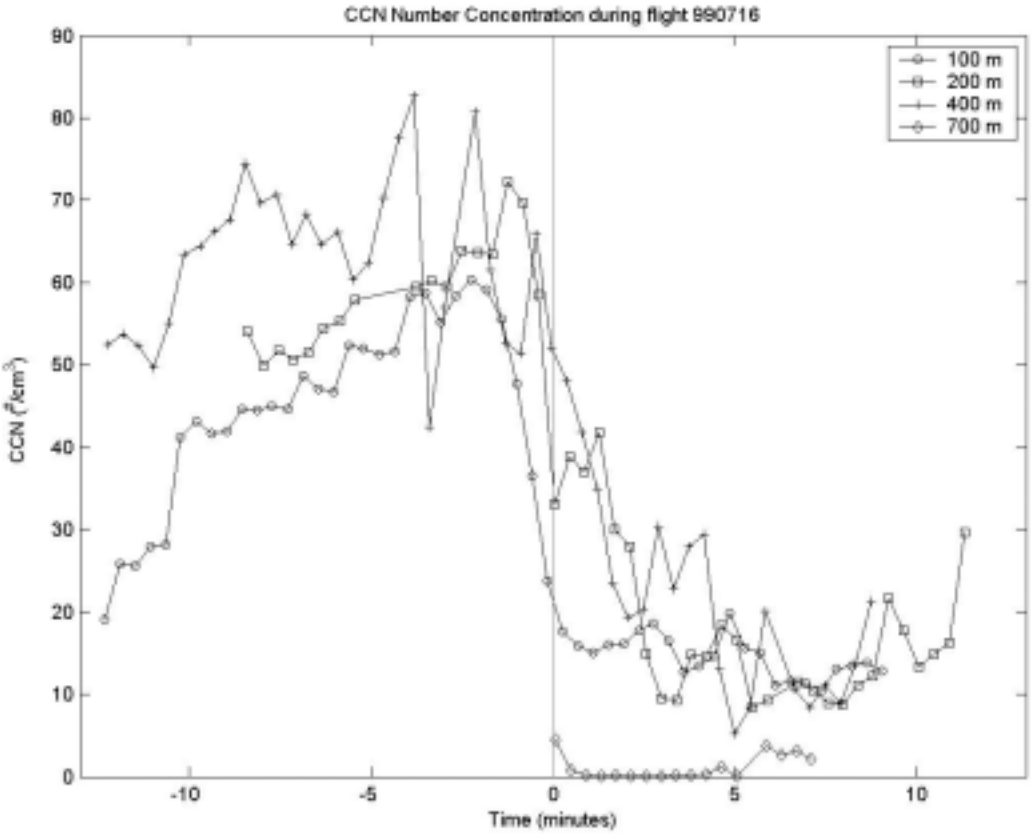

Figure 7. (a) Liquid water content for profiles. The horizontal dashed gray lines roughly mark cloud top and cloud base of the solid cloud. The gray line indicates the Moist Adiabatic Lapse Rate (MALR). (b) Liquid water content across the level legs. The vertical gray line indicates the border between the solid stratus deck and rift region.

7(a)

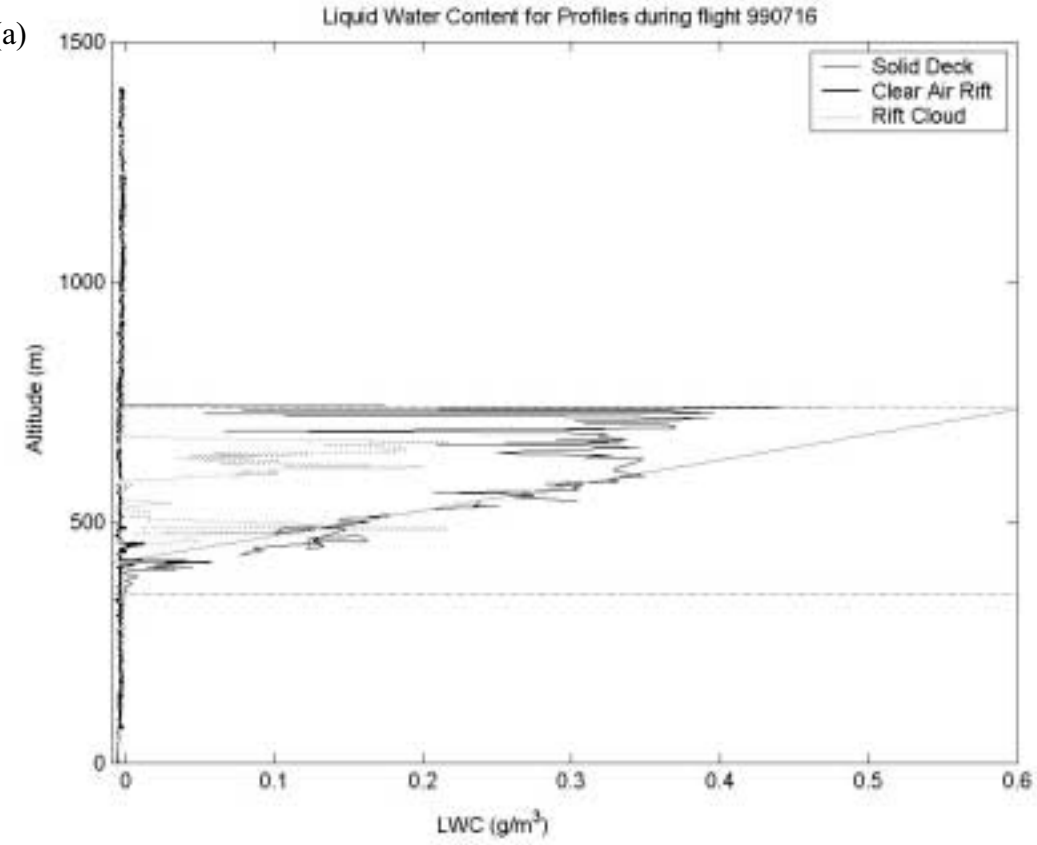

7(b)

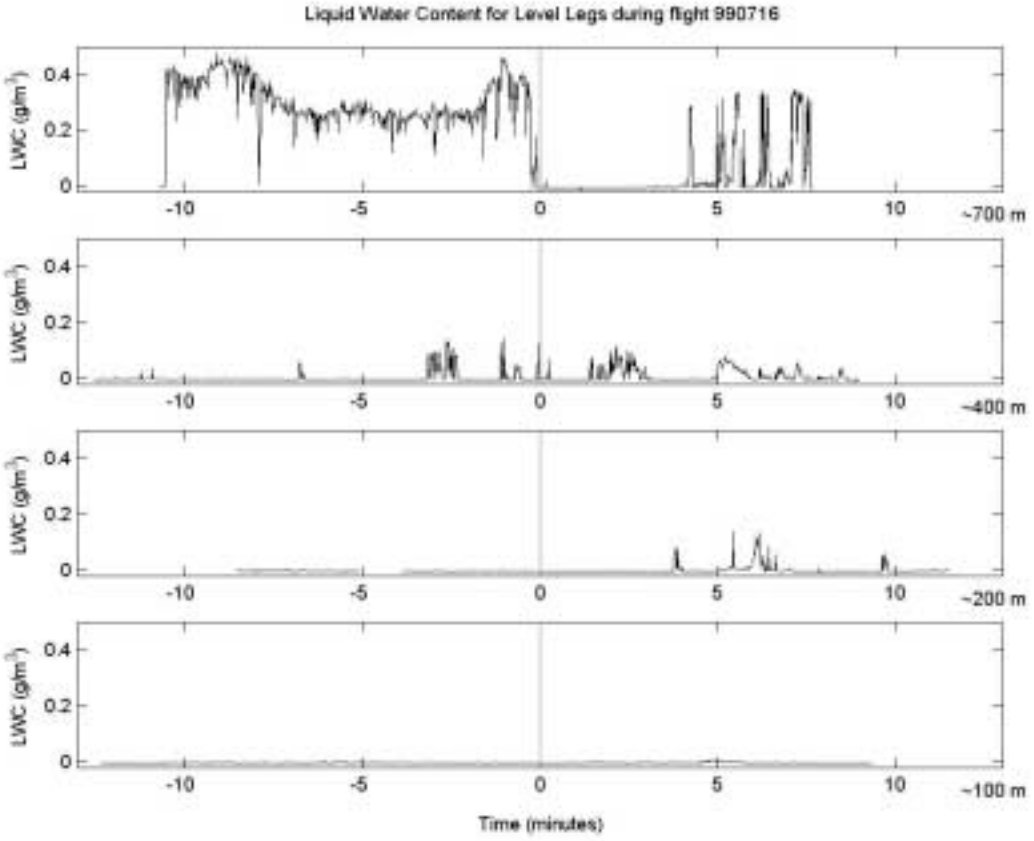
Liquid Water Content for Level Legs during flight 990716
LWC (g/m³)
0.4
0.2
0
-10
-5
0
5
10
~700 m
~400 m
~200 m
~100 m
Time (minutes)

Figure 8. (a) Drizzle Drop concentrations in the solid cloud (circle) and rift cloud (diamond) areas. The dashed gray lines roughly mark cloud top and cloud base of the solid cloud. (b) Effective diameter for cloud droplets in solid cloud and rift cloud areas. The dashed gray lines roughly mark cloud top and cloud base of the solid cloud. (c) Effective diameter for cloud droplets along the level legs. The vertical gray line indicates the border between the solid stratus deck and rift region.

8(a)

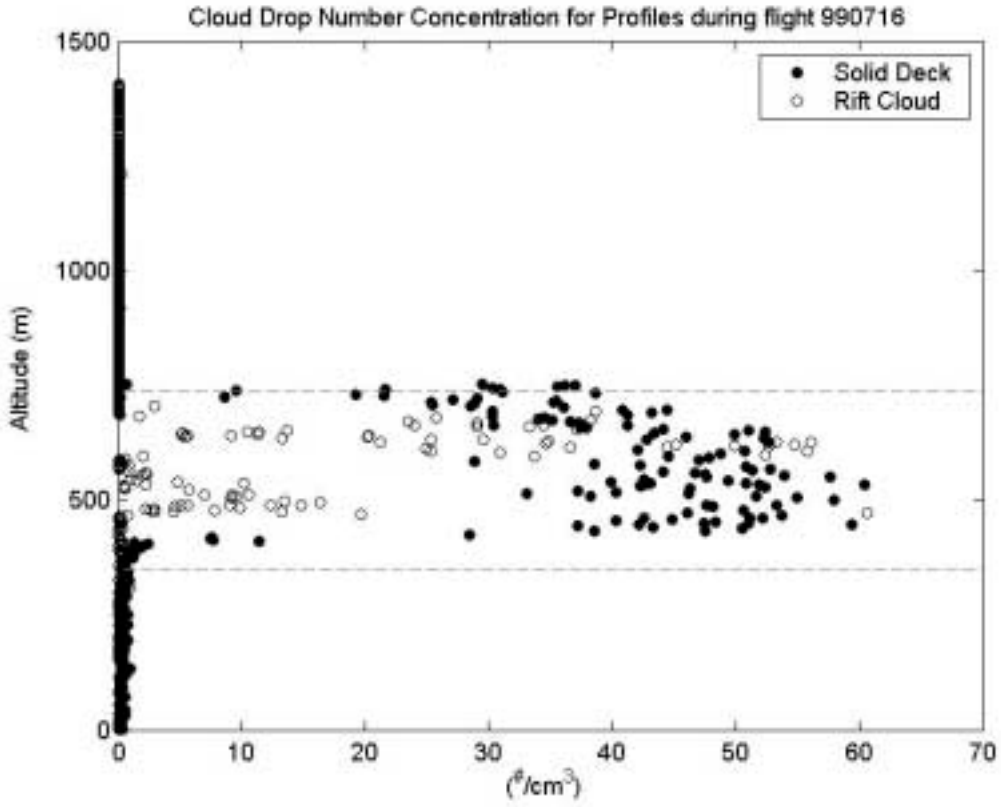

8(b)

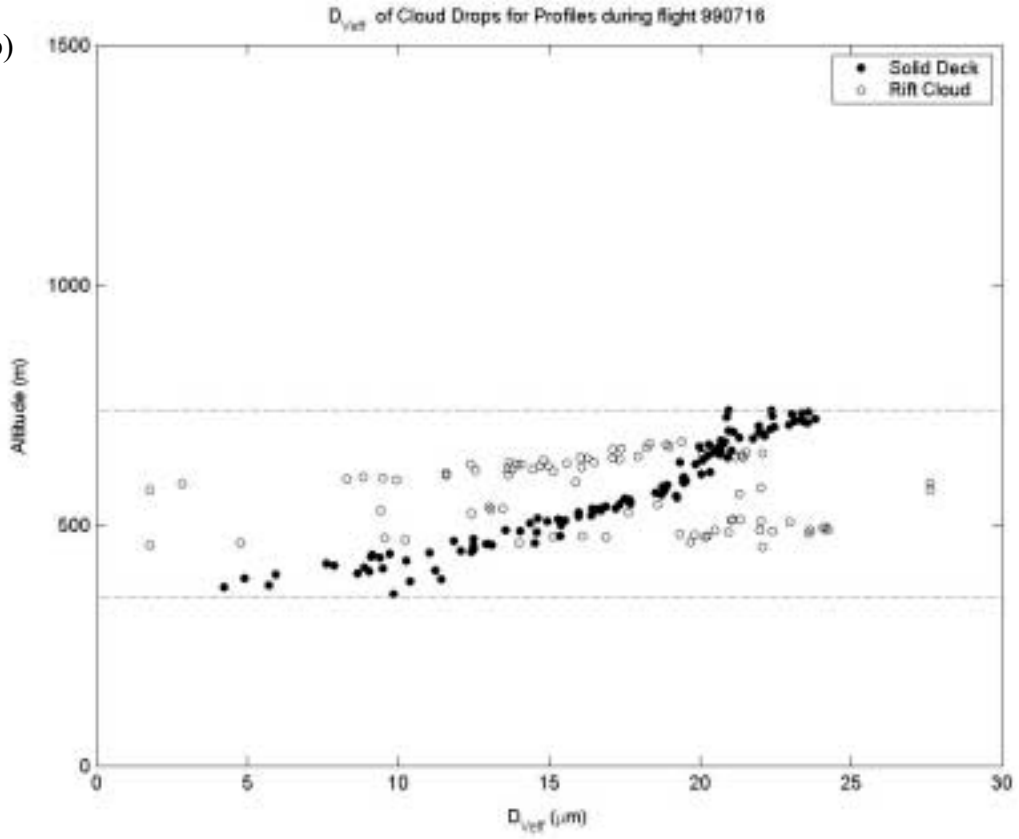
D_vef of Cloud Drops for Profiles during flight 990716
Solid Deck
Rift Cloud
Altitude (m)
D_vef (μm)
0
500
1000
1500
0
5
10
15
20
25
30

8(c)

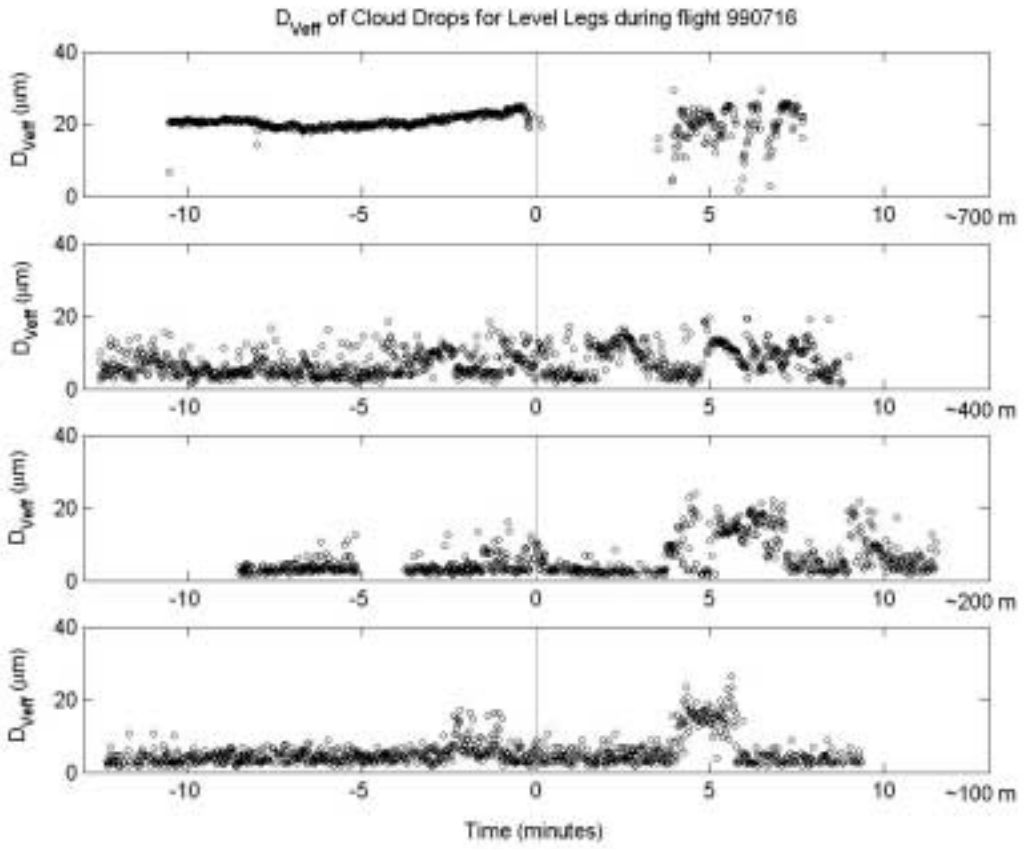
$D_{Veff}$ of Cloud Drops for Level Legs during flight 990716
$D_{Veff}$ (μm)
40
20
0
-10
-5
0
5
10
~700 m
~400 m
~200 m
~100 m
Time (minutes)

Figure 9. (a) Effective diameter for drizzle drops in the cloud profiles. The horizontal dashed gray lines roughly mark cloud top and cloud base of the solid cloud. (b) Effective diameter for cloud drops along the four horizontal legs. The vertical gray line indicates the border between the solid stratus deck and rift region.

9(a)

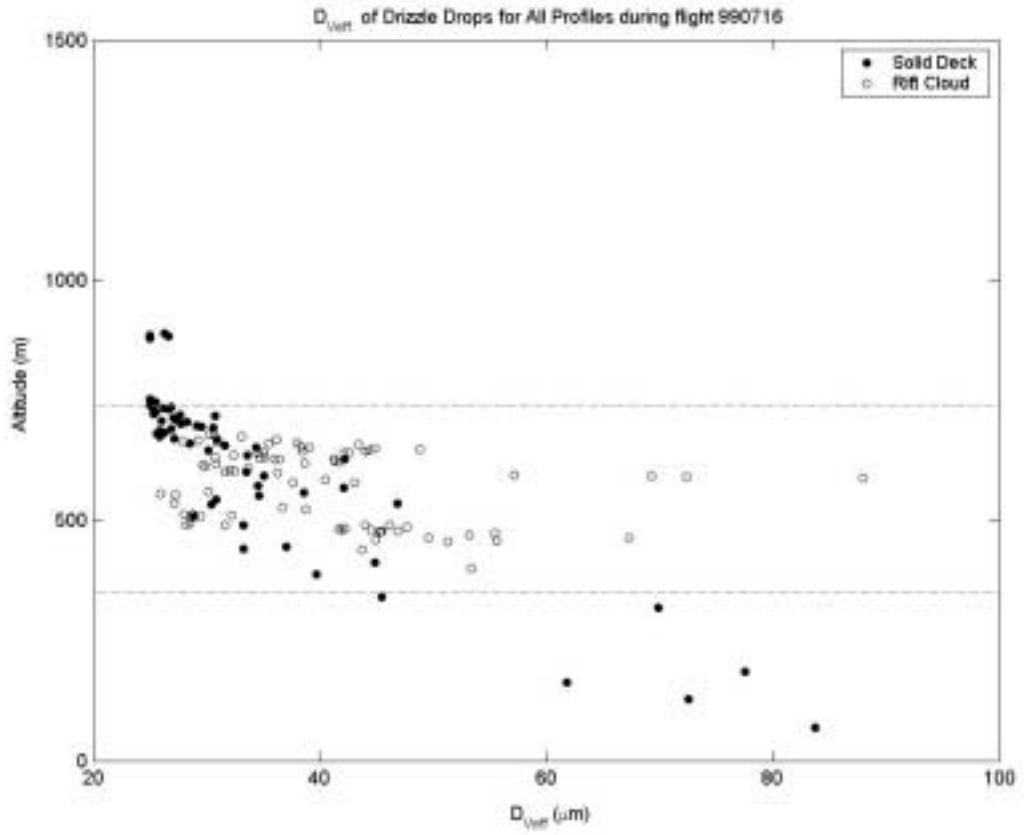

9 (b)

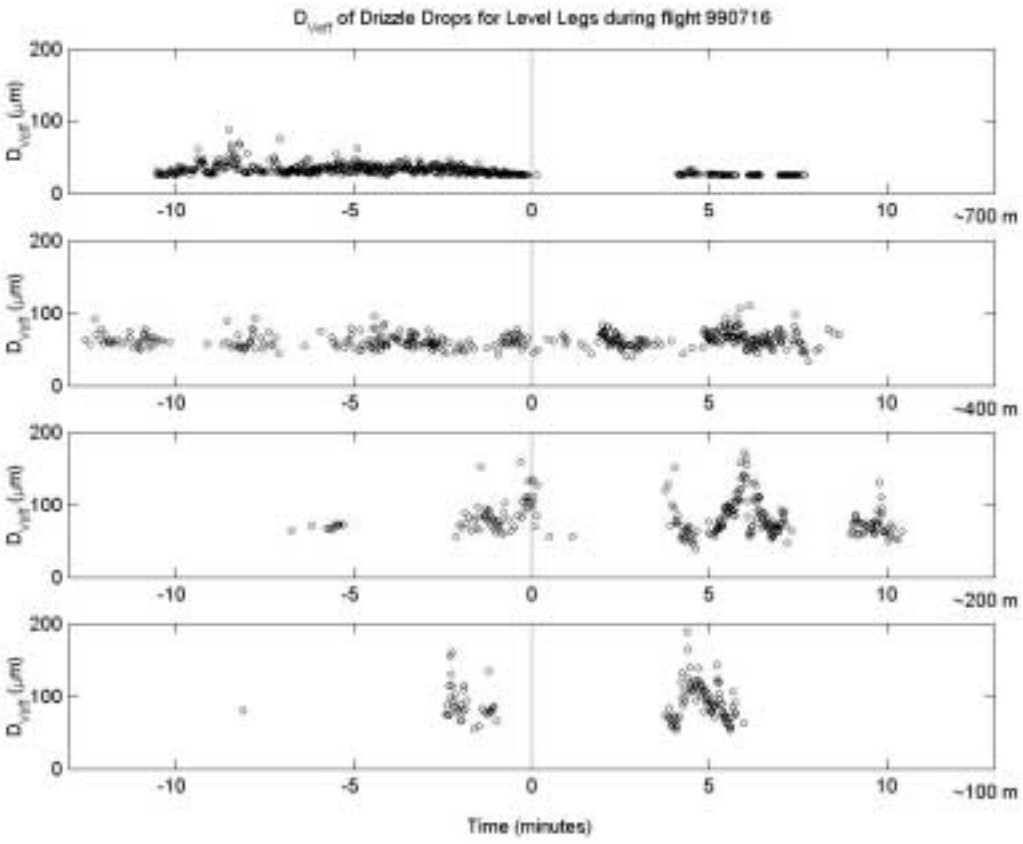
D_Vert of Drizzle Drops for Level Legs during flight 990716
D_Vert (μm)
200
100
0
-10
-5
0
5
10
~700 m
~400 m
~200 m
~100 m
Time (minutes)

Figure 10. Cloud and drizzle droplet spectra from the solid cloud deck (solid line) and the rift cloud (dotted line) regions. These spectra are based on approximately 5 sec averages. The cloud spectra were obtained at a height of about 75 m. Drizzle spectra were made below the cloud (at 75 m) in the two areas. The first bin of the drizzle spectra was eliminated due to instrument error of over counting the number of droplets (thus the gap in data between the cloud and drizzle drop spectra).

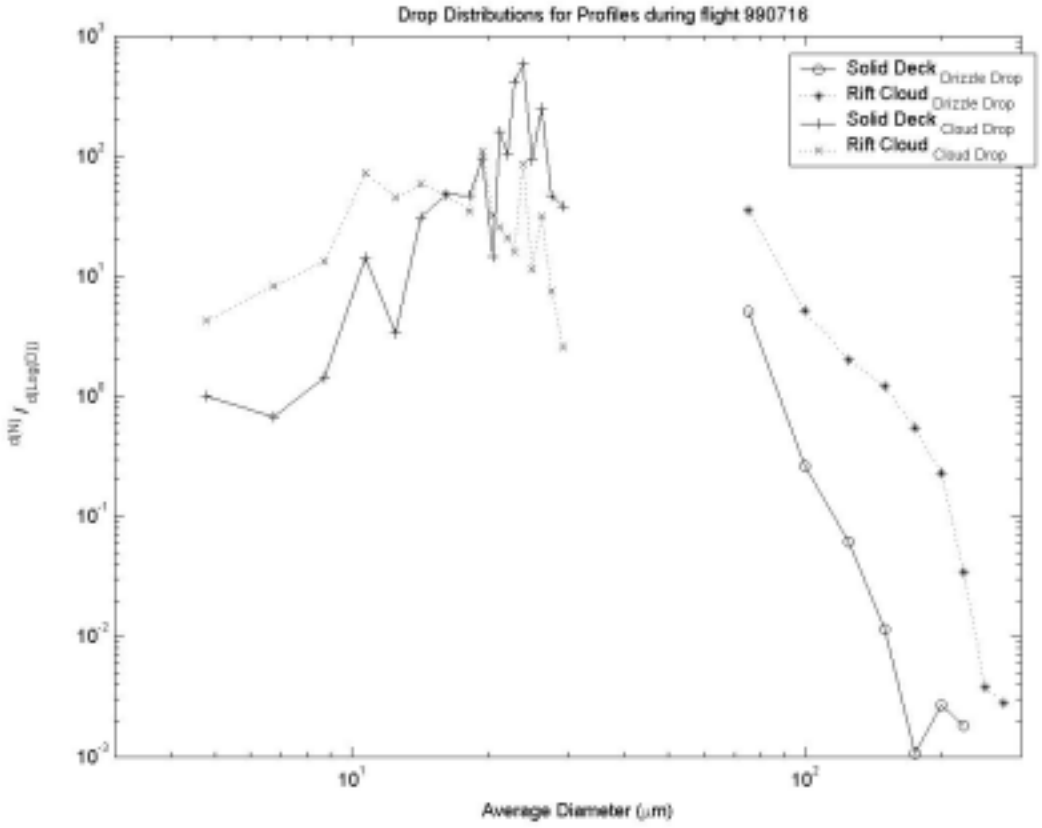

Figure 11. Schematic of possible cleaning mechanism associated with stratus deck.

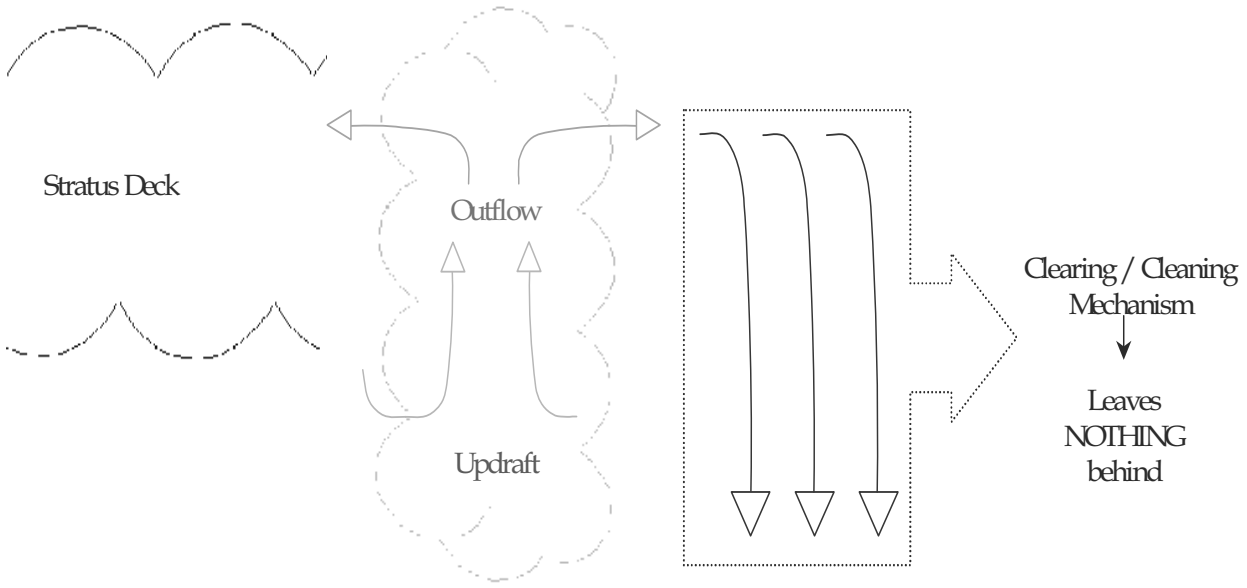

Figure 12. Radiative effective cloud droplet diameter derived from GOES-10 data off the coast of California during 16 July 1999 at (a) 1900 UTC and (b) 2100 UTC.

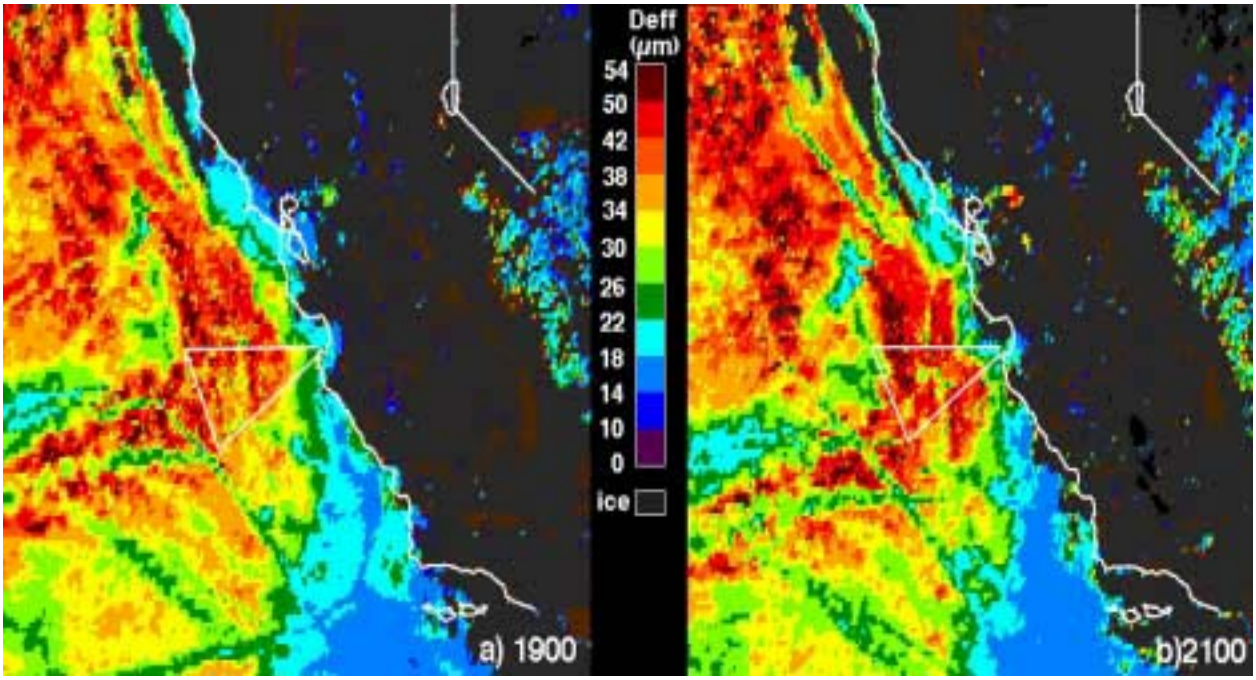

Figure 13. Microphysical differences from the C-130 and Electra aircraft flown on 30 June 1987.

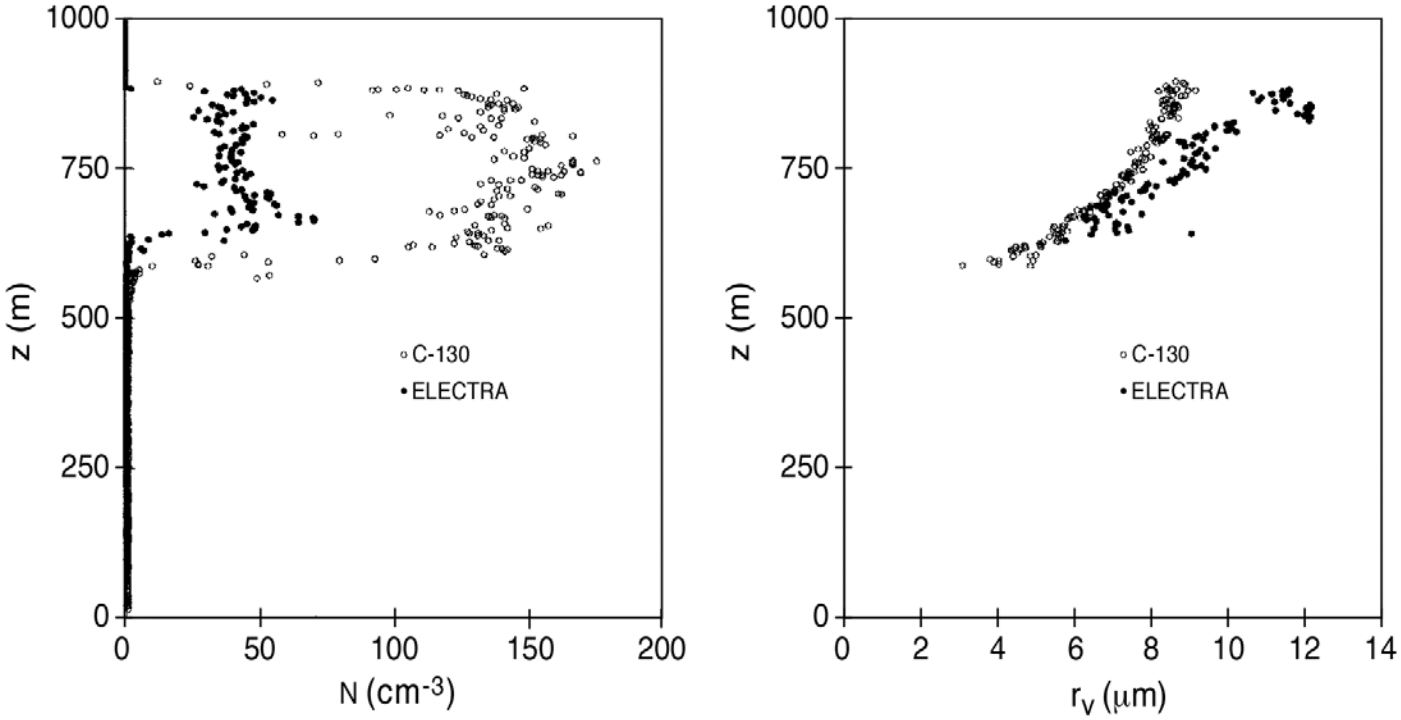

# Table Captions

Table 1. Summary of instruments used on the CIRPAS Airplane

Table 2. Summary of time and modification of time for Level Legs.

Table 3. Summary of solid deck, clear air rift and rift cloud droplet distributions in the sub-cloud layer (100 - 200 meters). The times encompassing the measurements of the legs are: - 1 to – 0.5 minutes represents the deck area, 0 to + 0.5 minutes is the rift area and + 5 to + 5.5 minutes is the rift cloud. See Figure __ for time location of times analyzed.

Table 4. Summary of solid deck, clear air rift and rift cloud droplet distributions in the lower cloud layer 400 - 500 meters). Details as with Table 3.

Table 5. Summary of solid deck, clear air rift and rift cloud droplet distributions in the upper cloud layer (600 - 700 meters). Details as with Table 3.

Table 1. Summary of instruments used on the CIRPAS Airplane

| Instrument | Function |
|---|---|
| GPS Systems | Measures GPS, position, speed and altitude. |
| Temperature | Rosemount sensor; range: -50 $^{O}$C to 50 $^{O}$C; resolution ~0.5 $^{O}$C. |
| Dew Point Temperature | Chilled mirror device; range: -50 $^{O}$C to 50 $^{O}$C; resolution ~0.5 $^{O}$C. |
| Sea Surface Temperature | Tasco Sensor. |
| Hot Wire Liquid Water Content | Liquid water vapor sensor. |
| Wind, 5 hole probe | Rosemount sensor; measures True Air Speed (TAS), mean wind, slip and attack angles. |
| Total Solar Radiometer | Measures solar radiation; range: 0.285 μm – 2.800 μm. |
| Cloud Imaging Probe (CIP) | Measures particle size distribution; used mainly for drizzle drops; 15 μm – 1550 μm range. |
| Forward Scatter Spectrometer Probe (FSSP) | Measures particle size distribution; used mainly for cloud droplets; 1.0 μm - 47.0 μm range. |
| Cloud Aerosol Scatterprobe (CAS) | Measures particle size distribution; used for particles falling within the 0.5 μm – 40 μm range. |
| Ultrafine Condensation Particle Counter (CPC) | Measures particle number concentration; range: $D_p$ > 0.003 μm. |
| CCN Spectrometer | Measures cloud condensation nuclei (CCN); range: 0.1 %< Supersaturation Condition < 2.0 %. |

Table 2. Summary of time and modification of time for Level Legs.

| | Leg at 100 m | Leg at 200 m | Leg at 400 m | Leg at 700 m |
|---|---|---|---|---|
| UTC at start of leg | ~ 1924 UTC | ~ 2004 UTC | ~ 2027 UTC | ~ 2052 UTC |
| UTC at border | ~ 1937 UTC | ~ 2016 UTC | ~ 2038 UTC | ~ 2102 UTC |
| Mission time at start | 8860 sec | 11260 sec | 12660 sec | 14160 sec |
| Modification of time | Leg – 9600 sec | 11950 sec - Leg | Leg - 13300 sec | 14770 sec - Leg |

Table 3. Summary of solid deck, clear air rift and rift cloud droplet distributions in the sub-cloud layer (100 - 200 meters). The times encompassing the measurements of the legs are: - 1 to – 0.5 minutes represents the deck area, 0 to + 0.5 minutes is the rift area and + 5 to + 5.5 minutes is the rift cloud. See Figure 2 for time location of times analyzed.

| | Solid Deck | | Clear Air Rift | | Rift Cloud | |
|---|---|---|---|---|---|---|
| | Profile | Leg | Profile | Leg | Profile | Leg |
| Ultrafine Particles ($cm^{-3}$) | 157 | 173 | 83 | 130 | 2069 | 98 |
| Aerosol (CAS) ($cm^{-3}$) (0.5–1μm) | 1 | 3 | 0 | 4 | 2 | 3 |
| CCN ($cm^{-3}$) | -- | 56 | -- | 29 | -- | 16 |
| Drizzle Drops (CIP) ($liter^{-1}$) | 7 | 20 | 0 | 5 | 0 | 143 |
| Drizzle LWC ($g\ m^{-3}$) | 0 | 0 | 0 | 0 | 0 | 0.1 |

Table 4. Summary of solid deck, clear air rift and rift cloud droplet distributions in the lower cloud layer 400 - 500 meters). Details as with Table 3.

| | Solid Deck | | Clear Air Rift | | Rift Cloud | |
|---|---|---|---|---|---|---|
| | Profile | Leg | Profile | Leg | Profile | Leg |
| Ultrafine Particles ($cm^{-3}$) | 101 | 159 | 273 | 310 | 635 | 120 |
| Aerosol (CAS) ($cm^{-3}$) (0.5–1μm) | 31 | 20 | 3 | 14 | 10 | 20 |
| CCN ($cm^{-3}$) | -- | 51 | -- | 48 | -- | 9 |
| Cloud Drops (FSSP) ($cm^{-3}$) | 37 | 23 | -- | -- | 6 | 29 |
| Drizzle Drops (CIP) ($liter^{-1}$) | 46 | 49 | 0 | 16 | 1055 | 130 |
| Dv effective cloud (μm) | 12 | 10 | -- | -- | 14 | 12 |
| Dv effective drizzle (μm) | 38 | 60 | -- | 52 | 46 | 70 |

Table 5. Summary of solid deck, clear air rift and rift cloud droplet distributions in the upper cloud layer (600 - 700 meters). Details as with Table 3.

| | Solid Deck | | Clear Air Rift | | Rift Cloud | |
|---|---|---|---|---|---|---|
| | Profile | Leg | Profile | Leg | Profile | Leg |
| Ultrafine Particles ($cm^{-3}$) | 205 | 1893 | 1683 | 1242 | 1754 | 763 |
| Aerosol (CAS) ($cm^{-3}$) (0.5–1μm) | 27 | 34 | 0 | 0 | 21 | 12 |
| CCN ($cm^{-3}$) | -- | 7 | -- | 3 | -- | 15 |
| Cloud Drops (FSSP) ($cm^{-3}$) | 42 | 33 | 0 | 0 | 23 | 10 |
| Drizzle Drops (CIP) ($liter^{--1}$) | 349 | 3350 | 0 | 14 | 1454 | 2326 |
| Dv effective cloud (μm) | 20 | 24 | -- | -- | 16 | 20 |
| Dv effective drizzle (μm) | 30 | 28 | -- | 26 | 36 | 26 |